MASTERARBEIT / MASTER'S THESIS

Titel der Masterarbeit / Title of the Master's Thesis

„Diffractive Light- and Neutron-Optical Elements of Varying Thickness from Stacks of Photosensitive Foil"

verfasst von / submitted by

Saba Shams Lahijani

angestrebter akademischer Grad / in partial fulfilment of the requirements for the degree of

Master of Science (MSc)

Wien, 2021 / Vienna, 2021

Studienkennzahl lt. Studienblatt / degree programme code as it appears on the student record sheet:	AU 066 876
Studienrichtung lt. Studienblatt / degree programme as it appears on the student record sheet:	Masterstudium Physik
Betreut von / Supervisor:	ao. Univ.-Prof. Dr. Martin Fally
Mitbetreut von / Co-Supervisor:	Dipl.-Ing. Dr. Jürgen Klepp

Acknowledgement

First and foremost, I have to thank my research supervisors, ao. Univ.-Prof. Dr. Martin Fally and Dipl.-Ing. Dr. Jürgen Klepp. They were always available whenever I had a question about my experiments or writing. Without their assistance in every step throughout the process, this master thesis could not be successful. A special thank goes to Dr. Friedrich-Karl Bruder for providing us with the needed material for our experiments.
I would like to thank my friend, Whitney, for her support.
I would also like to thank my mother, Parvin, and father, Hamid, as well as my brothers and other members of my family for providing me with unfailing support during my studies.
Finally, I must express my very profound gratitude to my husband, Hamed, for his patience, support and great love. He has encouraged me always to continue my way and work on the realisation of my dreams.

Contents

1 Introduction

1.1 Holography

The idea of holography was invented and developed by Dennis Gábor (1900–1979). If a coherent laser beam were split into two coherent partial waves, one of them would strike the photo plate after being reflected or scattered from the object (object beam), and another one came from the light source directly (reference beam) on the photo plate, they would interfere with each other and an interference pattern (interference fringes) would appear on the photo plate which is called "hologram". The information of the object wave is contained in the modulation of the brightness of the fringes and in the distance of the fringes.

Since Gabor's original paper [10] and the invention of the laser [20] various holographic procedures have been developed[12]. Holography is a two stage process. The first stage is the recording of the hologram in the form of an interference pattern. In the second stage, the hologram acts as a diffraction grating for the reconstruction beam, and the image of the object is reconstructed by the hologram.

1.1.1 Holographic Recording

The most important thing in holographic recording is the recording of both the phase and amplitude of the object wave. The phase of the wave cannot be recorded on the recording medium, therefore it should be converted to an intensity. With an interferometry technique, an unknown wavefront (object beam) can be added to a known wavefront (reference beam). Both object and reference waves can be written in general as (cf. [8] and [19])

$$\vec{S}(x,y) = e^{-i\Phi(x,y)}\vec{s}(x,y)\,, \tag{1}$$

$$\vec{R}(x,y) = e^{-i\Psi(x,y)}\vec{r}(x,y)\,. \tag{2}$$

Here $\vec{s}(x,y)$ and $\vec{r}(x,y)$ are the amplitudes of object and reference beam at superposition point, respectively. $\Phi(x,y)$ is the phase of the object wave and $\Psi(x,y)$ represents the phase of the reference beam. The intensity I is the square of the sum of the complex amplitudes, in which the dependency of I on the phase and amplitude of the object wave can be seen

$$\begin{aligned} I(x,y) &= \left|\vec{S}(x,y) + \vec{R}(x,y)\right|^2 \\ &= \vec{S}(x,y)\cdot\vec{S}^*(x,y) + \vec{R}(x,y)\cdot\vec{R}^*(x,y) + \vec{S}(x,y)\cdot\vec{R}^*(x,y) + \vec{R}(x,y)\cdot\vec{S}^*(x,y)\,. \end{aligned}$$

1.1.2 Hologarphic Reconstruction

By exposing the recording material to two beams in interferometer, the interference pattern begins to be formed. The completed interference pattern can transmit the light with a transmittance function t which depends on the intensity of the hologram (cf. [19])

$$t = \alpha I = \alpha\left(|\vec{s}(x,y)|^2 + |\vec{r}(x,y)|^2\right) + \alpha\left(\vec{S}(x,y)\cdot\vec{R}^*(x,y) + \vec{R}(x,y)\cdot\vec{S}^*(x,y)\right)\,. \tag{3}$$

To reconstruct the object wave, the hologram will be illuminated with the original reference beam. The reconstructed wave $\vec{P}$ is

$$\begin{aligned} \vec{P} &= t\vec{R} \\ &= \alpha\vec{R}(x,y)\left(|\vec{s}(x,y)|^2 + |\vec{r}(x,y)|^2\right) \\ &\quad + \alpha\vec{R}(x,y)\cdot\vec{R}^*(x,y)\cdot\vec{S}(x,y) + \alpha\vec{R}(x,y)\cdot\vec{R}(x,y)\cdot\vec{S}^*(x,y)\,. \end{aligned} \tag{4}$$

There are four terms on the right-hand side of Eq. (4): the first term is too small and negligible, the second term represents the attenuated reference beam. In the third term, the phase of the conjugate reference beam recorded in the hologram and the phase of the reconstruction beam cancel each other and the phase of the original object beam remains which results in the reconstruction of the image of the object. The fourth term represents the conjugate object beam which results in forming a conjugate image.

1.2 Different Types of Holograms

There are different types of hologram which can be used for different applications. Three holograms, i.e., transmission hologram, reflection hologram and Denisjuk hologram will be mentioned in next parts but we focused on the transmission holograms in this work extensively.

1.2.1 Transmission Hologram

The transmission holograms can be recorded using a laser. During the transmission hologram recording, the object and reference beams incident on the sample from the same side. They interfere with each other to make an interference pattern. The image is recorded in the interference pattern on the film, and can be reconstructed by shining the coherent light of a laser on the hologram. The image will be formed by transmitting a beam of light through the hologram. For these holograms, the recorded interference pattern is oriented perpendicular to the film's surface. These holograms are great at reconstructing the original wavefront but they are not very capable to filter the different wavelengths of light, therefore using a white light to reconstruct the original beam results blurriness in the hologram.

1.2.2 Reflection Hologram

In contrast to transmission hologram, the object and reference beam strike the sample from the opposite sides. These two beams interfere with each other to create an interference pattern which is oriented parallel to the film's surface. During the reconstruction process, the incident beam will be reflected from the hologram's surface so that the incident beam and reflected object beam lie on the same side of hologram.

1.2.3 Denisjuk Hologram

Denisjuk invented a simple method for making reflection hologram. The laser beam is fanned out by a convex lens and shines through the holographic film as a reference beam. Behind the film is the object which partially reflects the reference beam back to the film. The reference beam and the reflected object beam interfere with each other and an interference pattern will be made. To reconstruct the object beam a white light can be used as it is used for other reflection holograms.

1.3 Mach Zehnder Interferometer

To record a hologram an interferometer is needed. The Mach Zehnder interferometer is used for splitting the amplitudes of beams. It consists of two mirrors and two beamsplitters, so that the incoming beam in the interferometer is split in two beams. The transmitted and reflected beam will be reflected from the mirrors. Since these two beams travel the separate optical paths, a phase modulation will happen. We consider the electric fields of s-polarized transmitted $\vec{E_1}$ and reflected waves $\vec{E_2}$ at the position of the sample in the interferometer as follows (cf. [13])

$$\vec{E_1}(\vec{r},t) = \vec{E_{01}} e^{i(\vec{k_1}\cdot\vec{r}-\omega t)} = \vec{E_{01}} e^{i\phi_1} \,, \tag{5}$$

and

$$\vec{E_2}(\vec{r},t) = \vec{E_{02}} e^{i(\vec{k_2}\cdot\vec{r}-\omega t)} = \vec{E_{02}} e^{i\phi_2} \,, \tag{6}$$

where $\phi_1 = \vec{k_1}\cdot\vec{r} - \omega t$ and $\phi_2 = \vec{k_2}\cdot\vec{r} - \omega t$ indicate the phase of transmitted and reflected beams, respectively. Here, $\vec{E_{01}}$ is the amplitude of the transmitted wave and $\vec{E_{02}}$ is the amplitude of the reflected wave. The total electric field of the superimposed beam can be written as

$$\vec{E}_{total} = \vec{E_1}(\vec{r},t) + \vec{E_2}(\vec{r},t) = \left[\vec{E_{01}} e^{i(\vec{k_1}\cdot\vec{r})} + \vec{E_{02}} e^{i(\vec{k_2}\cdot\vec{r})}\right] e^{-i\omega t} \,. \tag{7}$$

The detectors are not able to measure the electric field directly, but it is the time averaged intensity of the light that can be observed experimentally. The time averaged intensity can be obtained by integrating of the electric fields over a time interval which results in

$$\langle|\vec{E}_1|^2\rangle = I_1 \,, \quad \langle|\vec{E}_2|^2\rangle = I_2 \,, \tag{8}$$

which in turn leads to

$$\begin{aligned} I_{total} &= \langle|\vec{E}|^2\rangle = \langle\vec{E}\cdot\vec{E}^*\rangle \\ &= \langle(\vec{E}_1+\vec{E}_2)\cdot(\vec{E}_1^*+\vec{E}_2^*)\rangle \\ &= \langle|\vec{E}_1|^2\rangle + \langle|\vec{E}_2|^2\rangle + \langle\vec{E}_1\cdot\vec{E}_2^*\rangle + \langle\vec{E}_2\cdot\vec{E}_1^*\rangle \,. \end{aligned} \tag{9}$$

and

$$\langle\vec{E}_1\cdot\vec{E}_2^*\rangle = \langle\vec{E}_{01}\cdot\vec{E}_{02}^*\rangle e^{i\left[(\vec{k_1}-\vec{k_2})\cdot\vec{r}\right]} = \sqrt{I_1 I_2}\, e^{i\left[(\vec{k_1}-\vec{k_2})\cdot\vec{r}\right]} \,, \tag{10}$$

$$\langle\vec{E}_2\cdot\vec{E}_1^*\rangle = \langle\vec{E}_{02}\cdot\vec{E}_{01}^*\rangle e^{-i\left[(\vec{k_1}-\vec{k_2})\cdot\vec{r}\right]} = \sqrt{I_1 I_2}\, e^{-i\left[(\vec{k_1}-\vec{k_2})\cdot\vec{r}\right]} \,. \tag{11}$$

For simplicity, the exponential term can be written in terms of cosine function

$$I_{total} = I_1 + I_2 + 2\sqrt{I_1 I_2}\cos\Omega \,, \tag{12}$$

where $\Omega = (\vec{k_1}-\vec{k_2})\cdot\vec{r}$ is the phase difference between two waves and the controlling factor of interference. It is clear from the form of (12) that it has a sinusoidal behaviour. Therefore, the refractive index of the interference pattern has a sinusoidal behaviour

$$n(\vec{x}) = n_0 + n_1 \cos\left(\vec{K}\cdot\vec{x}\right) \,, \tag{13}$$

where n_0 is the average refractive index, n_1 is the amplitude of the spatial modulation of the refractive index and $\vec{K}$ is grating vector (see section 2.2).

The maximum and minimum values of intensity will be obtained when $\cos\Omega = 1$ and $\cos\Omega = -1$, respectively. Therefore

$$I_{max} = I_1 + I_2 + 2\sqrt{I_1 I_2} \,, \tag{14}$$

and

$$I_{min} = I_1 + I_2 - 2\sqrt{I_1 I_2} \,. \tag{15}$$

The quality of the interference pattern (contrast of fringes) can be described by the visibility parameter $V(\vec{r})$ given by

$$V(\vec{r}) = \frac{I_{max} - I_{min}}{I_{max} + I_{min}} = \frac{2\sqrt{I_1 I_2}}{I_1 + I_2} \,, \tag{16}$$

which is bounded by 0 and 1 from below and above, respectively.

2 Kogelnik Theory

There are different methods for modeling and calculating the diffraction efficiency of thick holograms to see the efficiency of the holograms for reconstruction of object beam. Here the coupled wave theory which was developed by Kogelnik in 1969, is used. This section is mainly based on the work of Kogelnik [18].

2.1 Thickness Parameter of Grating

There are different definitions for thickness of grating. One of the practical definitions is clarified by [11], in which the thickness parameter ρ is defined as

$$\rho = Q'/2\gamma = \frac{2\lambda^2}{\Lambda^2 \epsilon_1}\,, \tag{17}$$

where

$$Q' = \frac{2\pi\lambda d}{\sqrt{\epsilon_0}\Lambda^2\cos\theta}\,, \tag{18}$$

and

$$\gamma = \frac{\pi\epsilon_1 d}{2\lambda\sqrt{\epsilon_0}\cos\theta}\,. \tag{19}$$

Here λ denotes the wavelength of the incident beam, Λ is the grating spacing and ϵ_0 is the average relative permittivity, ϵ_1 is the amplitude modulation of the permittivity, γ is the strength parameter, d is the thickness of the grating, and the θ is the angle of incident beam. The grating acts as a thick grating when $\rho \geq 10$.

2.2 Wave Theory for Thick Hologram Gratings by Kogelnik

The coupled wave theory can predict the maximum possible efficiencies of thick holograms and the angular and wavelength dependence of diffraction efficiencies close to the Bragg angle. We recall that for a grating, the incoming waves are reflected from the interference pattern which are separated by the grating spacing Λ. If the path difference of the reflected waves is equal to an integer multiple of the wavelength of incident beam (λ), then the waves interfere constructively (Bragg' law)

$$2\Lambda\sin\theta_B^{\mathrm{ext}} = m\lambda\,, \tag{20}$$

where θ_B^{ext} is the external Bragg angle and m is a positive integer.

This theory assumes monochromatic light strikes on the hologram grating at or near the Bragg angle which is polarized perpendicular to the plane of incidence. Only two waves: incoming reference beam "R" and outgoing signal beam "S" obey the Bragg condition approximately.

In the present work the fringes are oriented perpendicular to the plane of incidence and sample's surface normal. Moreover, the grating vector $\vec{K}$ with length of $|\vec{K}| = K = 2\pi/\Lambda$ is oriented perpendicular to the fringe planes. Wave propagation in the grating is described by the scalar wave equation

$$\vec{\nabla}^2 E + k^2 E = 0\,, \tag{21}$$

where E is the complex amplitude of the electric field and k is the propagation constant, which is spatially modulated and is related to the relative dielectric constant and the conductivity of the medium.

In this work it is assumed that the recording of the hologram takes only the form of a spatial modulation of the refractive index of the medium. The average absorption constant α and its modulation are zero. It is more convenient to use refractive index under the following condition

$$n_0 \gg n_1 \,. \tag{22}$$

Here, n_0 is the average refractive index, and n_1 is the amplitude of the spatial modulation of the refractive index. The coupling of two waves and an exchange of energy between them in grating is because of amplitude of the spatial modulation n_1. The electric field of superposition by two waves in grating is

$$E = Re^{-i\vec{\rho}\cdot\vec{x}} + Se^{-i\vec{\delta}\cdot\vec{x}} \,, \tag{23}$$

where $\vec{\rho}$ is the propagation vector of the reference wave before of coupling and $\vec{\delta}$ is the propagation vector of the diffracted wave which is related to $\vec{\rho}$

$$\vec{\delta} = \vec{\rho} - \vec{K} \,, \tag{24}$$

where

$$\vec{\rho} = \begin{pmatrix} \rho_x \\ 0 \\ \rho_z \end{pmatrix} = \beta \begin{pmatrix} \sin\theta \\ 0 \\ \cos\theta \end{pmatrix} \,, \tag{25}$$

$$\vec{\delta} = \begin{pmatrix} \delta_x \\ 0 \\ \delta_z \end{pmatrix} = \beta \begin{pmatrix} \sin\theta - K/\beta \\ 0 \\ \cos\theta \end{pmatrix} \,, \tag{26}$$

where $\beta = 2\pi n/\lambda$. In general, if the Bragg condition is not satisfied, the vectors $\vec{\rho}$ and $\vec{\delta}$ have different lengths, but if the incidence happens at the Bragg angle, then the length of both vectors is equal to β (see Fig. 1).

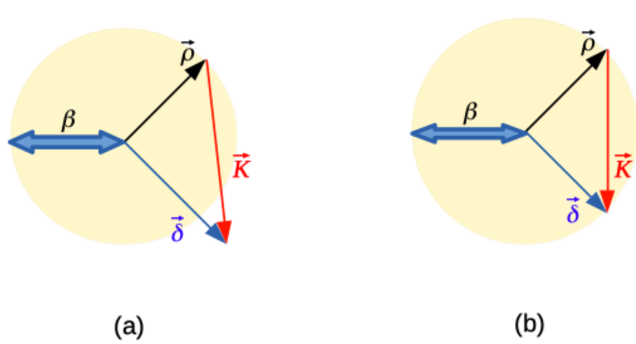

Figure 1: Wave vector diagram (Ewald sphere) (a) at near and (b) exact Bragg angle (see Eq. (24)).

If we set the length of $\vec{\rho}$ and $\vec{\delta}$ as β, we get the following result for Bragg condition

$$\cos\left(\frac{\pi}{2} - \theta_B^{\text{int}}\right) = \sin\theta_B^{\text{int}} = \frac{K}{2\beta} \,, \tag{27}$$

where θ_B^{int} is the internal Bragg angle. For a fixed wavelength the Bragg condition is violated by small angular deviations $\Delta\theta$ from the Bragg angle θ_B

$$\theta = \theta_B + \Delta\theta\,, \qquad \lambda = \lambda_B\,. \tag{28}$$

2.3 Diffraction Efficiency of Transmission Hologram

Solving the wave equation (21), in terms of R and S given in (23), by imposing the boundary conditions

$$R(0) = 1\,, \quad S(0) = 0\,,$$

one arrives at (see [18] for details)

$$R = e^{-i\xi}\left(\cos\sqrt{\xi^2+\nu^2} + \frac{i\xi}{\sqrt{\xi^2+\nu^2}}\cdot\sin\sqrt{\xi^2+\nu^2}\right)\,, \tag{29}$$

$$S = -ie^{-i\xi}\cdot\frac{\sin\sqrt{\nu^2+\xi^2}}{\sqrt{1+\xi^2/\nu^2}}\,, \tag{30}$$

where

$$\nu = \frac{\pi n_1 d}{\lambda\cos\theta}\,, \tag{31}$$

$$\xi = \frac{\vartheta d}{2\cos\theta}\,. \tag{32}$$

Here the dephasing measure ϑ in the coupled wave equation is given by

$$\vartheta = \Delta\theta\cdot K\cdot\cos\theta_B\,. \tag{33}$$

The diffraction efficiency η shows that how much the incident light power is diffracted into the signal wave. It is defined by

$$\eta = S(d)S^*(d)\,. \tag{34}$$

According to the data sheet of Bayfol foils used in this experiment [2], the diffraction efficiency of the hologram recorded on these foils are more than 95%. Hence, the diffraction efficiency of lossless dielectric gratings will be calculated. Finally, the diffraction efficiency of these gratings can be derived (see Fig. 2 below)

$$\eta = \frac{\sin^2\sqrt{\nu^2+\xi^2}}{1+\xi^2/\nu^2}\,. \tag{35}$$

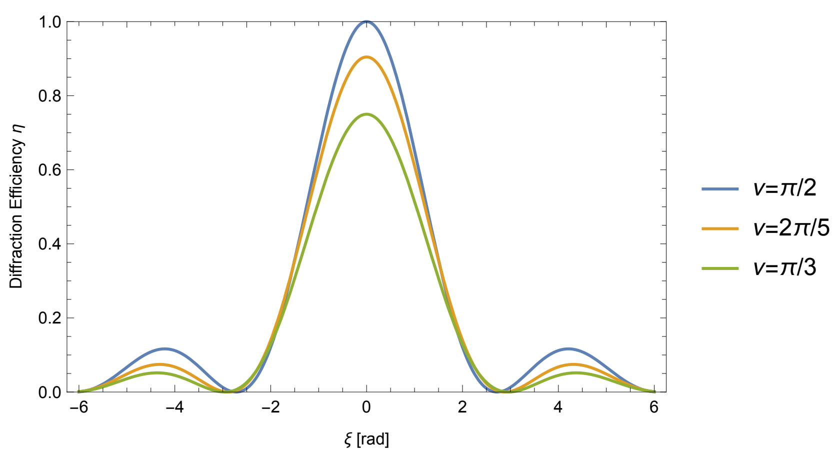

Figure 2: Diffraction efficiency as a function of ξ for three different values of ν.

3 Experiment

3.1 Material

The holographic film used in this experiment is Bayfol HX 200, a commercially available recording material for volume holography. Previous works on this material and its properties can be found in [3]. Most of the early holographic materials required wet-chemical or heat processing for formation a hologram after exposure to light while the Bayfol HX material can be recorded easily without any kind of these processings and shows a long term stability [5]. This material facilitates full color recording with low shrinkage (change in volume) after recording, although no chemical or heat processing is needed after recording [15]. To determine the optical properties of this film, some Denisyuk and 2-Beam reflection holograms were recorded on this material by the producer (Covestro). That is to say, this light-sensitive photopolymer film can be used to produce both reflection and transmission holograms. As we see the transmission spectrum of this material in Fig. 3, it can be recorded at different wavelengths between 440 nm and 680 nm in particular around 520 nm and 655 nm, while readout should ideally be carried out at about 570 nm. The Bayfol HX 200 consists of three

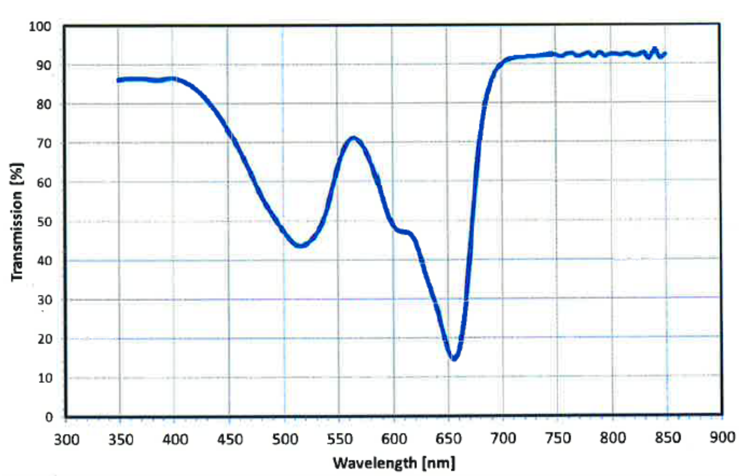

Figure 3: Transmission spectrum of Bayfol HX 200 [2].

layers:

- Protective cover film. It is a polyethylene film (PE) with 40 μm thickness. The cover film can be removed before recording (see 3.2).
- Light sensitive photopolymer with (16 ± 2) μm thickness and mean refractive index 1.505.
- Substrate. It is a cellulose triacetate film (TAC) with approximately (50 ± 2) μm thickness and refractive index 1.485.

3.1.1 Photopolymerization in Photopolymers

From the chemical point of view the raw material of the Bayfol film is composed of two different polymer chemicals: 1) The matrix precursors. The term matrix refers to a homogeneous and continuous material which provides a strong medium. A precursor in chemistry is

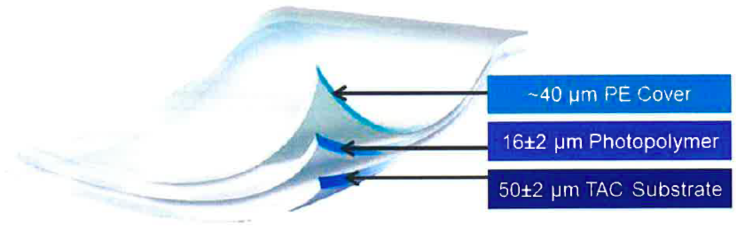

Figure 4: Bayfol HX 200 consists of three layers: 1) cover, 2) photopolymer, and 3) substrate [2].

a compound that participates in a chemical reaction that produces another compound. The matrix precursors are bonded during the film production and are responsible for the physical stability of the photopolymer. 2) The imaging components. They are responsible for the hologram formation during the exposure. The imaging components include polymerizable monomers and have abilities for absorbing the light and activating the polymerization.
In this experiment we recorded approximately sinusoidal interference patterns (see Section. 3.3.4). As a result, the refractive index will change sinusoidal when the photopolymer is exposed to the interference pattern. Then it triggers the monomers to start to be polymeized. The longer the exposure time, the more monomers are polymerized until no monomers are left. There are more polymarized monomers in the bright region than in the dark region. After a short period of time there is no more monomer in the bright region, therefore a monomer concentration gradient occurs between the bright and dark regions, so that the monomers diffuse from dark regions to the bright regions. The exposure with ligth can be continued until all the monomers are polymerized [2, 4].

3.2 Preparation of Samples

3.2.1 Pre-preparation

As mentioned above, the Bayfol HX 200 is very sensitive to light, therefore the films were prepared in a dark lab. At first we wanted to remove the cover layer from a piece of the foil material. Because the cover was thin and could not be too easily removed by hand, we decided to use adhesive band so that the adhesion between the adhesive tape and the cover can remove it from the photopolymer layer without applying any pressure or scratching on the latter. It was not possible to use tweezers because it could damage the material. Next step was to build a holder with round tips so that it would not tear the foil while holding it (see Fig. 5 and 6). The holder was built from a mounting base, a binder clip and a piece of paper just to keep the clip on the mounting base stable. It was difficult to remove the cover from the foil without light and without touching the foil. Therefore, we prepared all the necessary tools using for preparation before turning off the light. At first a lamp with red light was placed in about 1m distance from the preparation table. The lamp head was positioned lowly not to shine on the material directly. According to Fig. 3, a good choice would be a dim light with the wavelength about 560 nm, because the absorption of the Bayfol foil is low at this wavelength and the foils would not absorb prematurely. However there was no lighting with corresponding wavelength spectrum available. For shipment, the Bayfol foils were completely sealed in an aluminum envelope and packed in a white box. The box of sheets, a pair of gloves, a pair of scissors, an adhesive band and the binder clip mounting on a base were placed close to each other on the table before turning off the light. Wearing the gloves, the top of the aluminum envelope was cut with the scissors carefully so that the sheets would not tear. A small piece with size about $2 \times 2\ cm^2$ was cut with scissors and held with the holder described above (see Fig. 5) as a test sample to see if, for example, the cover layer can be identified by its color. We closed the aluminum package with adhesive tape, put it back in the white box and put it in a drawer not to receive any light or dust. We cut a piece of adhesive tape and attached it gently to the sheet. Then the sheet was held with two fingers without applying any pressure. The adhesive band was pulled back and then down, so that the cover layer was removed. The suspected cover layer and the rest consisting of photopolymer and substrate were laid on the table in full lighting. After one day, the part that changed color from blue to light purple was identified as photopolymer on substrate, the other part as the cover layer.

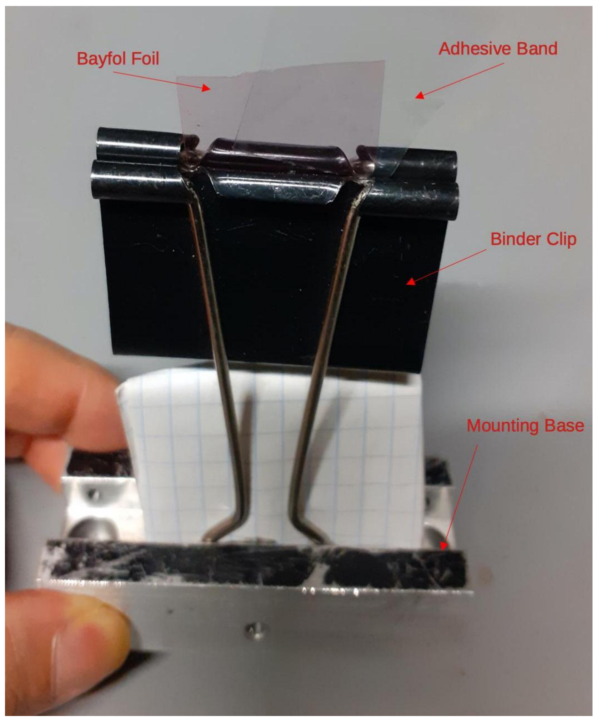

Figure 5: Preparation of foil samples, ready for recording: The foil is held with a binder clip on a mounting base.

3.2.2 Single Photopolymer Layer Hologram (PS)

The single photopolymer layer hologram consists of one layer of foil, i.e. of a photopolymer (p) and a substrate (s). (The single photopolymer layer hologram is referred to as PS hologram in the following). After removing the cover layer, the film with size of $2 \times 2cm^2$ was attached between two microscope glasses like a sandwich. The glasses were fixed together with glue and left in the black box at room temperature for one day to ensure adhesion.

3.2.3 Two Photopolymer Layer Hologram (SPPS)

To reach the high diffraction efficiency for light as well as for neutrons, we decided to double the thickness of photopolymer, because one can see from the diffraction efficiency's equation

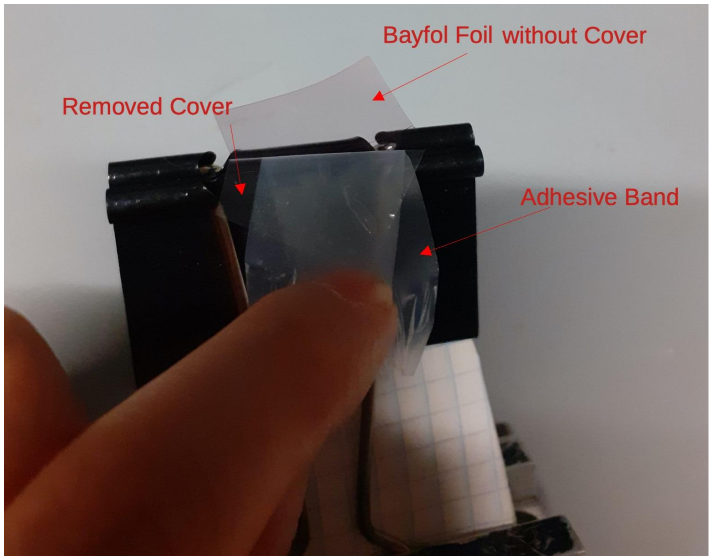

Figure 6: Preparation of films: The cover layer is removed from the foil by using an adhesive band (the photopolymer and the substrate layers cannot be separated).

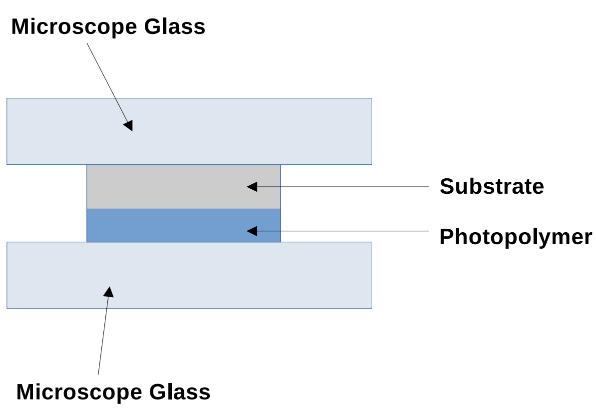

Figure 7: Schematic of PS sample.

from Kogelnik (see Eq. 35), by increasing the thickness of material, the diffraction efficiency will also increase. The SPPS hologram consists of two substrate layers (s) and in between there are two photopolymer layers (p). (The two photopolymer layer hologram in this design is referred to as SPPS hologram in the following). To prepare this sample, two small pieces of sheet with the size of 2×2 cm^2 were cut with scissors and put on a tissue. The cover of first sheet was removed while it was held by the binder clip. The photopolymer sticks a little bit to the hand after removing the cover. This stickiness property of photopolymer helps us to identify which layer it is, a photopolymer or a substrate. We put the sheet immediately on a microscope glass from the substrate side. The second sheet was attached from its polymer side to the polymer of the first sheet (one polymer after another) after removing its cover. The sheets were sandwiched between two microscope glasses. The glasses were fixed with glue together and left in the black box for one day.

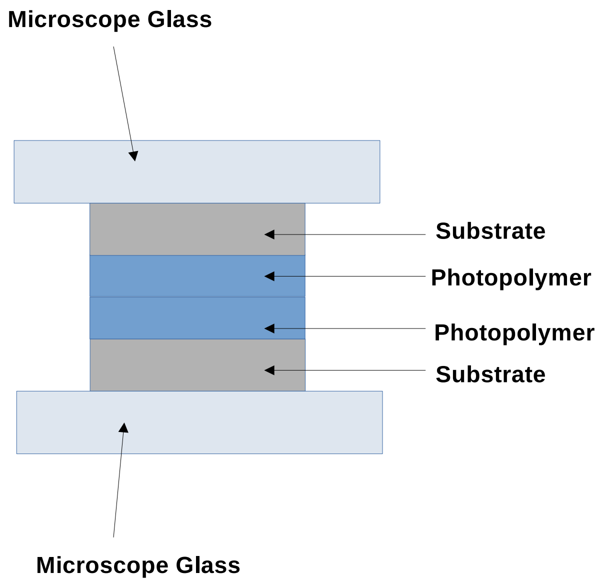

Figure 8: Schematic of SPPS sample.

3.2.4 Two Photopolymer Layer Hologram (PSPS)

The major idea was to increase the thickness of sample further more but we figured out it is not possible to have a stratified sample with three photopolymer layers one after another because there is a substrate in between which is not separable from the photopolymer. Since the diffraction properties of the stratified gratings consisting of recording layers with buffer layer in between, were studied before by [14, 22], a two photopolymer layer hologram with another design from SPPS hologram was prepared. It consists of two substrate layers (S) and two photopolymer layers (P). In this design, two small pieces of sheet with the size of 2×2 cm^2 were cut with scissors and put on a tissue. After removing the cover of first sheet, the first photopolymer layer was put on the microscope glass from its polymer side after removing the cover. Then the cover of next sheet was removed and the sheet was put on the substrate of the first sheet so that the polymers did not stick to each other. The sheets were sandwiched like the other samples between the two microscope glasses. The glasses were fixed together with glue and the sample was left in the black box for one day. (The two photopolymer layer hologram in this design is referred to as PSPS hologram in the following)

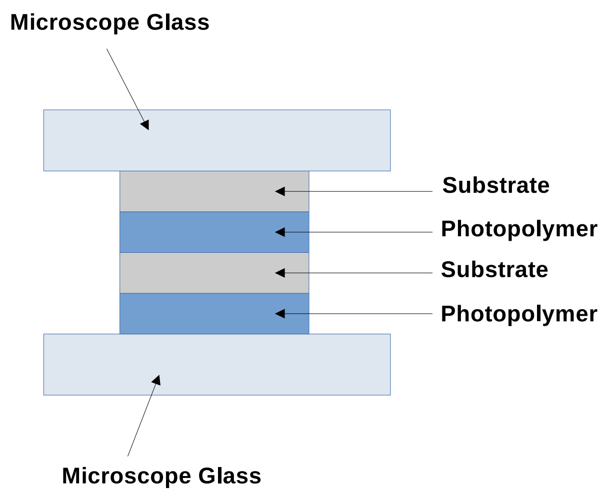

Figure 9: Schematic of PSPS sample.

3.3 Setup

3.3.1 Setup for the Recording the Holograms

The setup for recording the holograms consists of several parts. These parts and their principles will be explained in detail in the following

1. Laser,
2. Beam expander part,
3. Mach-Zehnder interferometer,
4. Sample holder.

3.3.2 Laser

The semiconductor laser Genesis MX SLM from Coherent with the $\lambda = 514$ nm and diameter $= 1$ mm is used for recording[6]. It provides up to 1 W power of visible green laser light.

3.3.3 Beam Expander

To illuminate the sample completely with a collimated and clean beam, a beam expander was used between the laser and the interferometer. By using a beam expander we could throw out the wave components caused by e.g. dust to get a plane wave approximately. There is a polarizer in front of the laser to make sure that the laser beam is linear and s-polarized. Then the laser beam goes through the beam expander part. In this part, two lenses are placed in a line on an optical rail. The first one is an objective lens with 5X magnification and focal length $= 25.4$ mm. The second one is a plano convex lens with focal length $= 200$ mm (see Fig. 10). The objective lens focuses most of the incident laser light onto a single spatial position (the focal point of the lens). It is the property of a positive convex lens to transform a single incident k-vector to a single point in space (the lens does a Fourier transform, see [12], for instance). However, due to imperfections of the laser output or dust particles in the beam path, the beam contains more than a single k-vector component. A pinhole is adjusted between two lenses at the position of the focal point of lenses, so that all the light that is focused at the focal point can pass the pinhole's opening. The small part of the incoming light that is not focused exactly at the focal point, but directed to a position at the optical axis slightly in front of or behind the pinhole, or even to an off-axis position, will be absorbed by the pinhole material. Thus, the wave expanding just behind the pinhole is transformed into a larger-diameter parallel beam that will contain only one single k-vector component, in good approximation. Therefore, it can be viewed as a good approximation to a plane wave and enables cleaner hologram recording. The diameter of the pinhole can be calculated [7]

$$D = \frac{\lambda f}{r}\,, \tag{36}$$

where D is the diameter of pinhole, f the focal length of the objective lens and r the radius of input beam to lens. In this experiment, the pinhole has the diameter of about 50 μm. The cleaned output beam from beam expander has the s-polarization state as the outgoing beam from laser.

A shutter is placed after the beam expander to be opened for a defined time for recording.

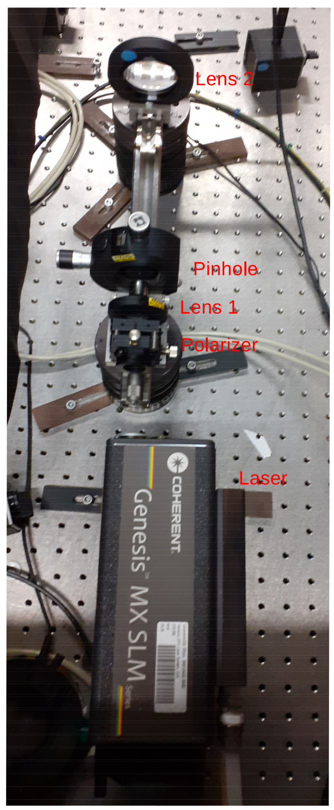

Figure 10: Beam expander from above.

3.3.4 Mach Zehnder Interferometer

In the Mach Zehnder interferometer (see Fig. 11), the laser beam goes to the beam splitter (BS) and is split in two coherent beams. The reflected and transmitted beams from the BS go to the mirrors (M_R and M_L) traveling different optical paths. The vertical zones of two beams will interfere with each other within the sample material after reflecting from the mirrors. We consider the electric fields of s-polarized transmitted $\vec{E}_1$ and reflected waves $\vec{E}_2$

at the position of sample in the interferometer as follows [13] We will reach the maximum contrast in fringes when the intensity of both beams are equal and both of the beams are s-polerized at the sample position. Therefore the power of both transmitted P_L and reflected beams P_R were measured with a LabMaster photometer close to the sample position. Because the power of the reflected beam was much higher than the transmitted beam, two polarizers were used to reduce the intensity of the beam (cf. Fig. 11). According to Malus's Law, when a linear polarizer is placed in a polarized beam of light, the intensity of the beam passing through the polarizer is [13]

$$I = I_0 \cos^2 \theta \,. \tag{37}$$

Here, I_0 is the intensity of the initial beam and θ refers to the angle between the polarization direction of initial beam and the axis of the polarizer. The reflected laser beam was vertically polarized. So, we rotated the first polarizer at an arbitrary angle different from 0° relative to the incident polarization direction. The second polarizer was put after the first one so that the polarization direction was set back to vertical. One can see in the Tab. 1 that the power of the reflected beam is lower than the transmitted beam after using the polarizers (a 50 : 50 ratio was desirable), but the visibility of the interference pattern is equal to 0.96 according to the Eq. (16) which is enough high and satisfying for the experiment. We chose

P_L (mW)	P_R (mW)	λ (nm)
3.58	1.72	514

Table 1: The measured power of transmitted (P_L) and reflected beams (P_R) at the sample position using the polarizers.

the θ_{ext} in Fig. 11, so that we could get out a grating spacing Λ about 500 nm according to the Eq. (20).

3.3.5 Sample Holder

The sample holder (Fig. 12) is an one-axis translation mount (model: XF50/M of Thorlabs) that can travel 50 mm along the lateral axis. A sample with maximum 4 mm thickness can be placed in this holder and carefully fixed by plastic-tip screws.

3.3.6 Recording the Holograms

To avoid the undesirable vibrations coming from air conditioner, train's movement near the lab, etc, it is important to record the holograms on an optical table which is isolated against such vibrations. The optical table is mounted on vibration isolation support legs (usually on air springs) to dampen vibrations. The compressed air in the legs of the table was once removed to investigate its influence on the hologram quality. By removing the air from the legs of the table, the table comes down and can not be isolated from the vibrations. The diffraction efficiency became smaller, because the vibrations affected the recording of hologram. So, the experiments leading to the results stated in this thesis were done on the table with filled air springs.
The LabMaster photometer was placed at the position of sample to measure the total power at the sample. The diameter of the photometer was $d_3 = 0.9$ cm while the diameter of

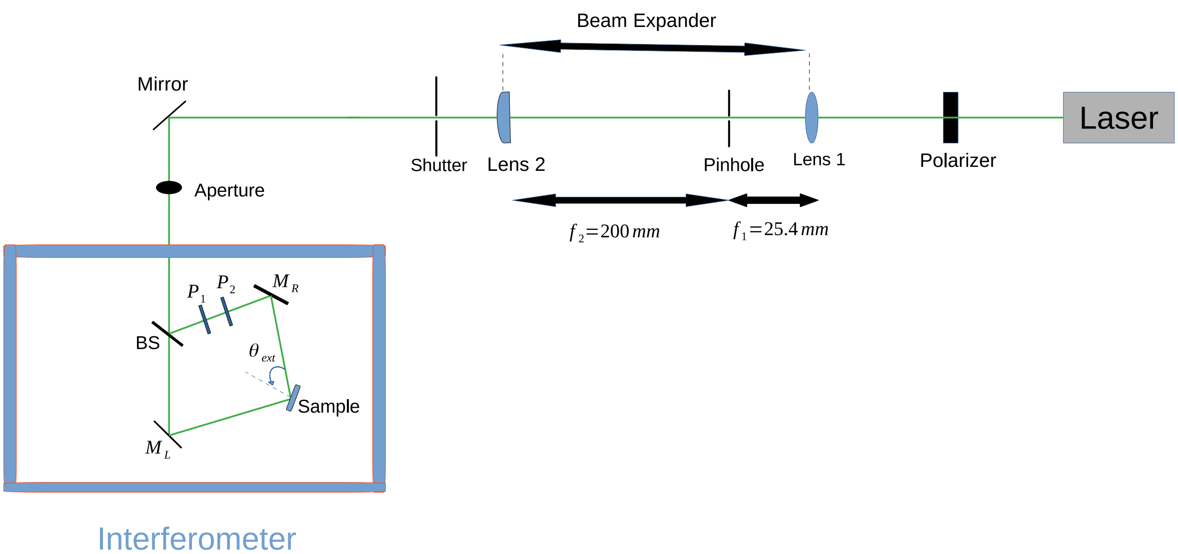

Figure 11: Setup for the recording. A green laser with $\lambda = 514$ nm and a diameter of about 1 mm was used for recording. The laser beam was checked with a polarizer to make sure it is s-polarized. Here the beam expander consists of lens 1 with $f_1 = 25.4$ mm, lens 2 with $f_2 = 200$ mm and a pinhole with $D = 50$ μm which is placed between the lenses at their focal point. In the interferometer, two polarizers P_1 and P_2 were placed on the right path between beam splitter (BS) and the mirror (M_R) to reduce the intensity of the reflected beam from BS. Both laser beams on the right and left arms of the interferometer are s-polarized at the sample position.

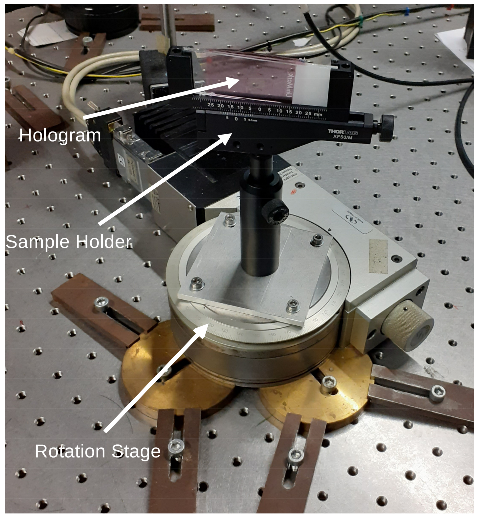

Figure 12: Sample holder. A one-axis translation mount was used as the sample holder which can travel 50 mm along the lateral axis. The sample holder is placed on a motorized rotation stage.

laser beam at the sample was $d_2 = 1$ cm. Therefore we converted the measured values by photometer with diameter of $d_3 = 0.9$ cm to the values for laser beam with the diameter of $d_2 = 1$ cm. Then we started the recording with a total power of laser 13 mW and a recording time of 5 s. Then we reduced the power and increased the recording time to keep the total dosage (E_{total}) constant approximately, because we wanted to record the holograms with the same recording's conditions (dosage and recording time). The intensity of laser reduces when it goes through the beam expander, therefore we measured the intensity of laser at the position of sample.

Time(s)	$P_{total} = P_R + P_L$ (mW)	E_{total} (mJ)	Intensity (mW/cm^2)	λ (nm)
5	1.48	7.40	1.48	514
10	1.11	11.1	1.11	514
15	0.74	11.11	0.74	514
20	0.74	14.8	0.74	514
25	0.49	12.34	0.49	514

Table 2: Recording time, total power of laser at the sample position (P_{total}), total dosage of laser at the sample position (E_{total}), and the total intensity at the sample position for recording.

The diffraction efficiencies of these holograms were measured to find out how they behave (see Fig. 13). As mentioned before, it is assumed that there is not any absorption in the holograms and the whole power of incoming beam is transferred to the diffracted beams. So the experimental form of diffraction efficiency (the diffraction efficiency is referred to as DE in the following) was used

- DE of −1st order:

$$DE_{-1} = \frac{I_{-1}}{I_{total}} = \frac{I_{-1}}{I_{-1} + I_0 + I_{+1}}\,, \tag{38}$$

- DE of the forward diffracted light:

$$DE_0 = \frac{I_0}{I_{total}} = \frac{I_0}{I_{-1} + I_0 + I_{+1}}\,, \tag{39}$$

- DE of +1st order:

$$DE_{+1} = \frac{I_{+1}}{I_{total}} = \frac{I_{+1}}{I_{-1} + I_0 + I_{+1}}. \tag{40}$$

They are the only DEs we observed. We also checked if there were any higher orders. From the DE's plots, we got the external Bragg angle $\theta_B \simeq 40°$. One can see according to the Bragg's law (see Eq (20))

$$\sin\theta^{ext}_{\pm m} = \pm\frac{m\lambda}{2\Lambda} = \pm\frac{m \cdot 633}{2 \cdot 500} > 1\,, \tag{41}$$

as soon as the $m \geq 2$, the higher orders will not appear. According to the results, the DE of the hologram recorded with $E_{total} = 7.4$ mJ was too small due to an unknown mistake (see Fig. 13). We decided to record a hologram with a total dosage between 7.4 mJ and 11.1 mJ to see the value of diffraction DE. A hologram with the recording time 11 s and the power 3.08 mW was recorded. Its DE reached 0.94. It seemed that the recording time 11 s was appropriate. That was the reason for recording another hologram with exactly $t = 11$ s but higher power $P = 5.3$ mW (all the powers of laser were measured at the sample position). Therefore the recording time $t = 11$ s and power of laser $P = 5.3$ mW ($P = 26$ mW at the laser) was set for recording the holograms (Tab. 3).

Time(s)	$P_{total} = P_S + P_R$ (mW)	E_{total} (mJ)	Intensity (mW/cm^2)	λ (nm)
11	3.08	33.88	1.48	514
11	5.3	58.3	5.3	514

Table 3: Recording time of $t = 11$ s, total power of laser at the sample position (P_{total}), total dosage of laser at the sample position (E_{total}), and the total intensity at the sample position for recording.

3.3.7 Setup for Readout the Holograms

A He-Ne laser ($\lambda = 633$ nm) with low intensity was used for readout (see Fig. 14). The intensity did not destroy the holograms to a degree noticeable after repeated readout attempts. Here no beam expander was used. A mirror for redirecting the laser to the sample

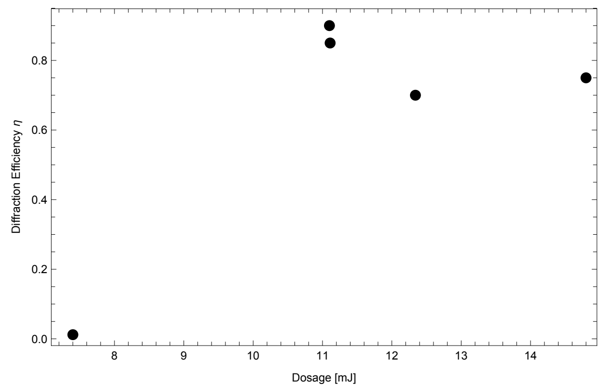

Figure 13: Diffraction efficiency of five holograms as a function of total dosage.

was used (because of the space limitations). To detect the intensity of diffracted beams, one photodiode (model: "Series 5T" of Centronic) was used which was connected to an amplifier. The amplifier was calibrated for the used wavelength. Then the amplified signal was measured by a digital multimeter readout automatically by a computer.

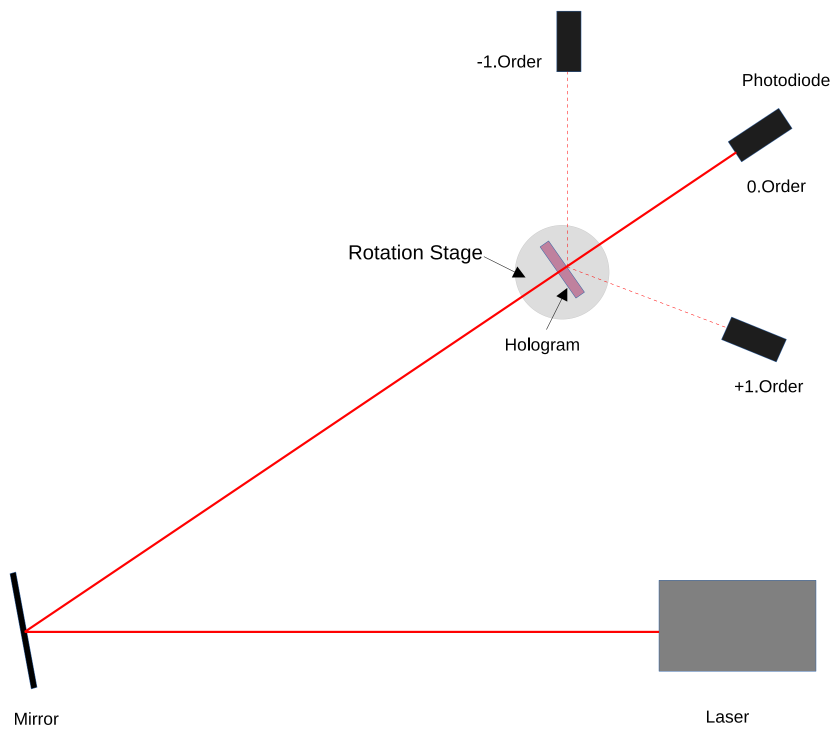

Figure 14: Readout-setup. A red laser beam is redirected by a mirror to the hologram. The hologram is put on a rotation stage. By rotating the hologram, the diffraction spots will appear at Bragg or near Bragg angle. A photodiode is placed behind the hologram to detect the forward diffracted beam (0th order). Then we moved the photodiode at the position of 1st Bragg diffraction order to measure its intensity. After that we placed the photodiode at the position where the −1st Bragg diffraction order appeared.

3.3.8 Readout of the Holograms

The polarization of the light was checked to make sure if it is s-polarized. By rotating the grating, the diffraction spots will appear if the Bragg's condition is obeyed, i.e., at Bragg and near the Bragg angle. The sample was rotated from 0° to 70° to find the position of the Bragg diffraction order. The photodiode was placed at a distance of about 20 cm behind the sample at the positions where the diffraction spots appeared. The angular dependency of the diffraction efficiency had broad peaks at the Bragg angle. The measurement of the intensity of each order and its side maxima(spanning more than 10°) was divided into several smaller parts helping us to detect the entire angular dependency. Such procedure is necessary for measuring broad peaks or the full angular dependency, because the actual positions where diffraction spots occur can deviate substantially from what is expected from estimations based on Bragg's law only [9]. For far off-Bragg angular positions, the diffracted beam will move away from the photo diode. The part of the sample hit by the laser must be the same for all rotation angles. So, care needs to be taken in advance that the sample position on the sample holder is such that the investigated sample part is positioned exactly at the position of the motor rotation axis.

4 Results

We succeeded in recording three holograms of type PS, SPPS and PSPS (see sections 3.2.2, 3.2.3 and 3.2.4). To characterize the holograms and find their effective thickness, the amplitude of the spatial modulation of the refractive index (n_1) and the grating spacing (Λ), the experimental data was compared with the model predictions by parameter fitting. The fitting program was written in Mathematica. The holograms were characterized by measuring the angular dependence of the diffraction efficiency (rocking curve). During the experiments there was not any changes in both recording and readout setups. To obtain the rocking curve of each sample, the intensity of the diffracted beams around the Bragg angle were measured (see section 3.3.8 by step-wise variation of the sample rotation angle (external angle of incidence). The diffraction efficiency of the diffracted beams for all measured diffraction orders were calculated using QtiPlot (open source data analysis software) by using the experimental form of DE (see section 3.3.6). The rocking curve for each hologram is shown in the following. Each of the holograms was measured in two separate times in July 2019 and January 2020.

4.1 Single Photopolymer Layer Hologram (PS)

The DE of three Bragg diffraction orders as a function of external rocking angle for PS hologram that were measured in July 2019 and January 2020 are shown in Fig. 15 and Fig. 16, respectively. As expected, there are maxima at the angles corresponding to the ±1st Bragg orders with a DE of about 0.9 at the angles of −40° and 40°, respectively. The minima of the DE almost reach zero, which suggests that the grating strength is approximately constant along the full thickness of the sample [25]. The DE decreases as the sample rotates far away from the ±1st Bragg orders, as expected. According to the Kogelnik theory (see Eq. (32) and Fig. 2) the angular distance $\Delta\theta$ between the two minima neighboring the central maximum can be calculated. One can see in Fig. 2 that the DE reaches its maximum value when $\xi = 0$, i.e., at the Bragg angle. The angular position neighboring the central maximum, where $DE = 0$, is found when the argument of the sine function in Eq. (35) is equal to π, i.e. $\sqrt{\nu^2 + \xi^2} = \pi$. By substituting the ν and ξ from Eqs. (31) and (32) in this relation and considering that $n \gg n_1$ (see definitions in section 2.2), we get

$$\Delta\theta \approx \frac{2\Lambda}{d}\,. \tag{42}$$

The grating spacing Λ can be calculated from Bragg's law (Eq. (20)). Because the Kogelnik theory works with internal angles, the external Bragg angles θ_B^{ext} in all our data plots must be transformed into internal Bragg angles θ_B^{int} by using Snell's law

$$n_a \sin\theta_B^{ext} = n_g \sin\theta_B^{in} = n_p \sin\theta_B^{int}\,, \tag{43}$$

where the refractive index of air is $n_a = 1$, the refractive index of microscope glass is n_g and the refractive index of photopolymer is $n_p = 1.505$. Here θ_B^{in} represents the internal Bragg angle in glass and θ_B^{int} is the internal Bragg angle in photopolymer. The Bragg equation (Eq. (20)) for θ_B^{int} can be written as

$$2\Lambda \sin\theta_B^{int} = \frac{\lambda}{n_p}\,, \tag{44}$$

where $\lambda = 633$ nm. Substituting the values of λ and θ_B^{int} in above equation leads to $\Lambda = 470 \pm 0.5$ nm. We calculated the error for Λ by using the Gaussian error propagation. Now we can calculate $\Delta\theta$ from Eq. (42) which gives $\Delta\theta \approx 3.32°$ for this sample. The angles at the minima around the maxima of DE in Fig. 15 and 16 were determined using QtiPlot and transformed in internal angles. The distance between two minima is $\Delta\theta \approx 3.65°$ and coincides with its value calculated from (42). For this hologram only the $\pm$1st Bragg orders were observed. The Bragg's law for second Bragg order ($m = 2$) is: $2\Lambda \sin\theta_B^{ext} = m\lambda = 2\lambda$. By substituting the values of Λ and λ we get $\sin\theta_B^{ext} > 1$ which is impossible. The high DE of this hologram shows that it can convert the incident light into the useful reconstructed wave very well. On the other hand, the DE of this sample measured in 2020 is as high as in 2019. In fact it is demonstrated that we are able to record an elementary hologram using Bayfol photopolymer. It is clearly seen that the hologram has not decayed substantially on a timescale of about half a year. Endurance is important for potential applications in light- and neutron-optics. If appropriate, the Kogelnik's calculation was used for the fitting model (see Eq. (35)). As mentioned in section 2.2, this theory works with internal angles while all the angles which were measured in this experiment are external. The corresponding experimental and fit results for the single photopolymer layer hologram are shown in Fig. 17. To find the best agreement of experimental and fit data, theleast squares method was used. According to this method, if the squared difference between an observed value, and the fitted value provided by a model reaches its minimum value, an appropriate fit can appear. Here, the fit leads to $n_1 = 0.015100 \pm 0.000025$ which agrees well with the recorded value in Bayfol foils stated in [2]. It is obvious that the uncertainty estimated by the program is probably too small and would increase substantially when including more samples of the same kind in the analysis. According to [2], the amplitude of modulation of the refractive index of a transmission hologram varies between 0.005 and 0.020. The effective thickness of PS hologram from fit is $d = 15.652 \pm 0.016$ μm and satisfying. The effective thickness value of this hologram is practically equal to the thickness of photopolymer (16 μm). The fit gives us also the value of $\Lambda = 493.321000 \pm 0.000017$ nm. The thickness parameter for this hologram can be found by using the Eq. (17). In this case $\rho = 218.072$ which is much larger than 10, therefore it is well justified to use the Kogelnik's calculation for the fitting, but comparing the data (black points) with the obtained fit functions, it is clear that the Kogelnik function cannot account for the slight asymmetry of the diffraction patterns. Also, the maxima neighboring the central peak are not well captured. The reason for this observation could be adjustment errors during the measurement.

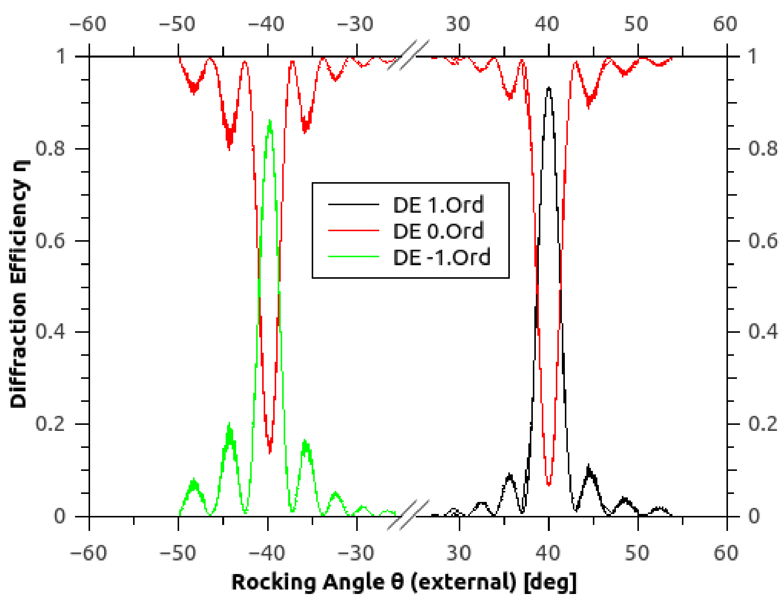

Figure 15: PS hologram (measured in 2019): -1st, 0th and $+1$st order rocking curves (green, red and black curves, respectively) as a function of external angle. One can not see a signal on the left side between $-60°$ and $-50°$ and the right side of the rocking curve between $50°$ and $60°$ because the intensity of the diffracted beams at these positions were very small in comparison to the other positions. Furthermore, there is a small asymmetry in peak heigth of the $\pm$1st order peaks, which is less pronounced in Fig. 16. The reason might be an adjustment error in photodiode positioning.

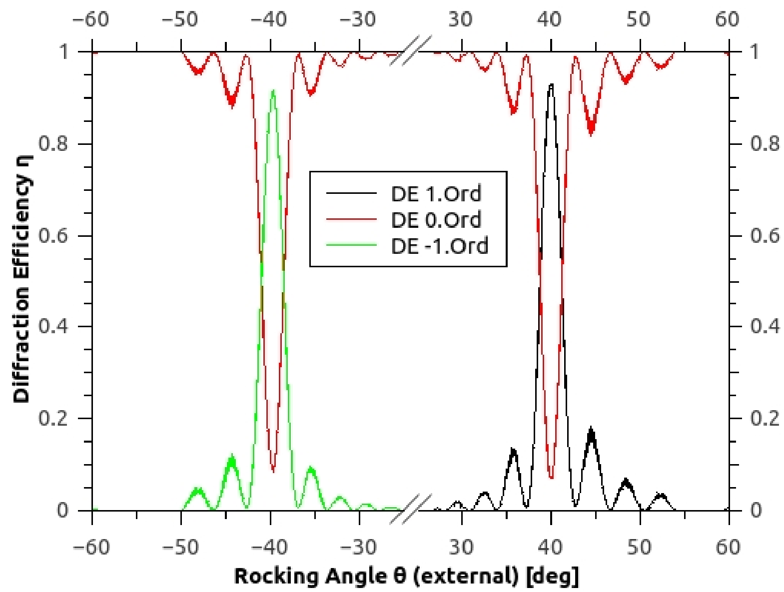

Figure 16: PS hologram (measured in 2020): −1st, 0th and +1st order rocking curves (green, red and black curves, respectively) as a function of external angle. One can not see a signal on the left side between −60° and −50° and the right side of the rocking curve between 50° and 60° because the intensity of the diffracted beams at these positions were very small in comparison to the other positions. The reason might be an adjustment error in photodiode positioning.

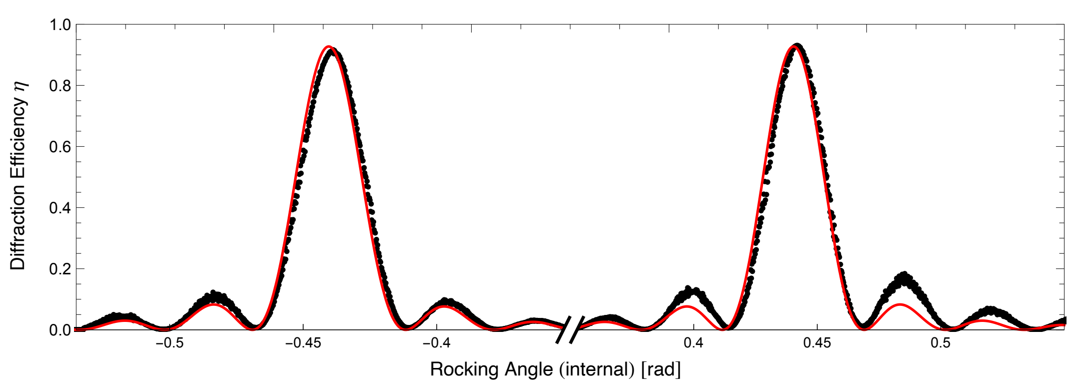

Figure 17: PS hologram: experimental data (black points) and the fit data (red solid curve). By rotating the sample, the existence of higher Bragg orders was checked but only the ±1st orders appeared as expected.

4.2 Two Photopolymer Layer Hologram (SPPS)

The grating is structured as described in section 3.2.3 and sketched in Fig. 8 is effectively a single photopolymer layer hologram with double thickness of a single photopolymer layer. As the results show in Fig. 18 and 19, there are more oscillations around the $\pm$1st Bragg diffraction orders and the frequency of these oscillations is higher than that of PS hologram. Here the DE of both observed diffraction orders has two maxima which are not at the Bragg position. The DE at the central peak (at the $\pm$1st Bragg angles) is smaller and the peaks beside it go up which is a sign of so-called overcoupling. According to the Eq. (35), the central peak of DE increases as the argument of the sine function approaches $\pi/2$ and decreases again for the argument increasing further ($\nu > \pi/2$). As can be seen from the equations for ν (see section 2.2), such oscillations of the peak of DE may occur due to variation of the grating "strength" (n_1), the thickness or the incident wavelength. For illustration, the behavior is shown by plotting theory curves following Eq. (35) for various values for the thickness d in Fig. 20. In comparison to PS hologram the DE of SPPS hologram is obviously smaller and

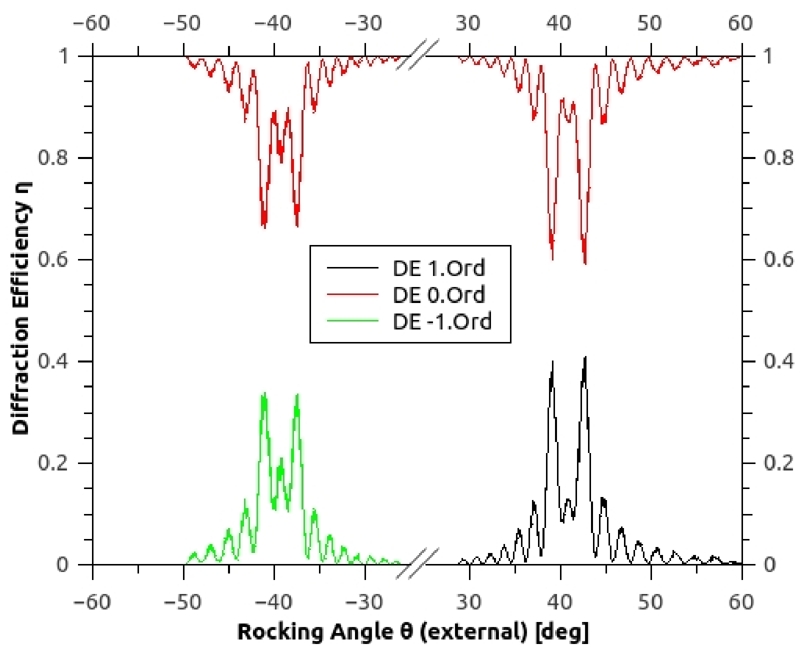

Figure 18: SPPS hologram (measured in 2019): $-$1st, 0th and +1st order rocking curves (green, red and black curves, respectively) as a function of external angle. Here one can see a slight asymmetry between the $\pm$1st diffraction orders. The photodiode might not be adjusted at the correct position to detect the diffracted beams.

the minima of some oscillations do not reach the zero point. There can be different reasons for that: 1) This may be attributed to the absorption of the grating. The grating might be not pure refractive index hologram. 2) Maybe the refractive index modulation decays with the depth in the sample [25]. It means the grating does not fulfill entirely the assumptions of the Kogelnik theory. The rocking curves of $\pm$1st Bragg diffraction orders are not symmetric because one can see in Fig. 21 and 22 that the maxima of DE for $\pm$1st Bragg diffraction orders are not identical. The internal angular distance between two minima neighboring the $\pm$1st order is about 1.5° which is in acceptable agreement with the calculated value from Kogelnik theory $2\Lambda/d \simeq 1.6°$ and it is smaller than the corresponding value for the PS

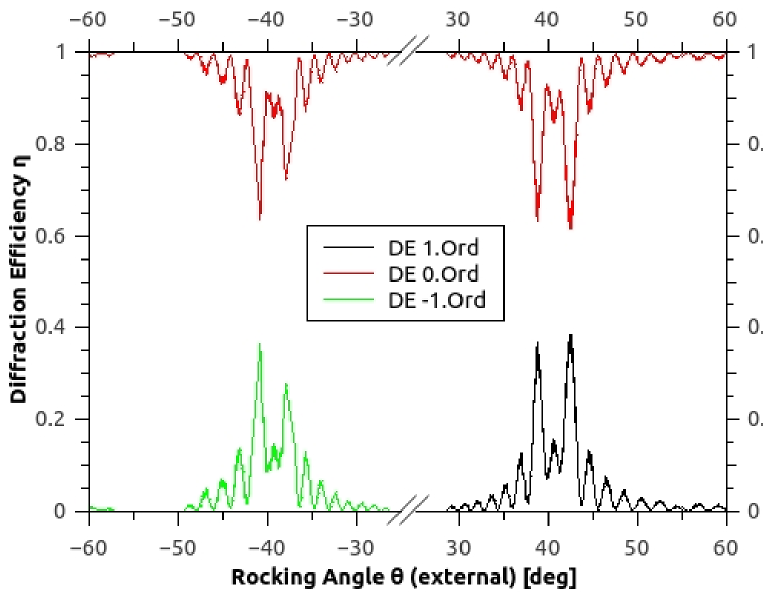

Figure 19: SPPS hologram (measured in 2020): −1st, 0th and +1st order rocking curves (green, red and black curves, respectively) as a function of external angle. Here one can see a slight asymmetry between the ±1st diffraction orders. The photodiode might not be adjusted at the correct position to detect the diffracted beams.

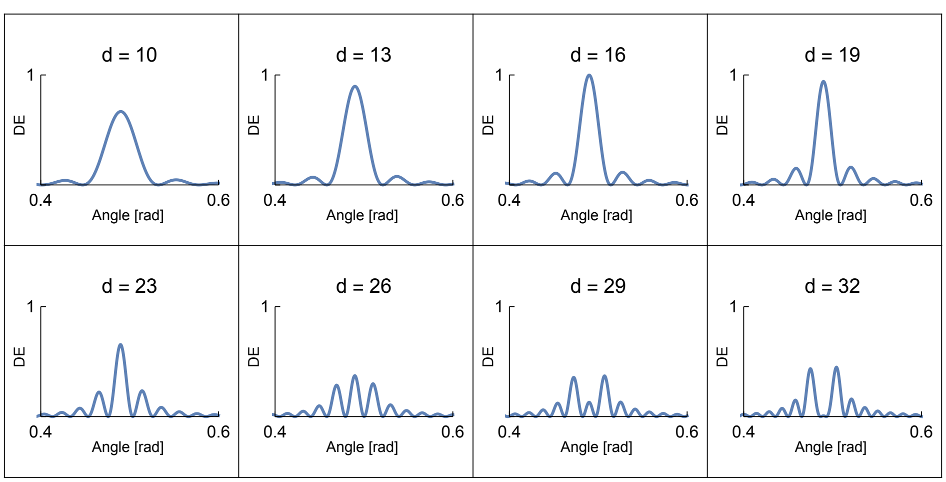

Figure 20: Diffraction efficiency of 1st order of a grating with increasing thicknesses according to Eq. (35).

hologram, because d of the SPPS grating is two times larger than that of the PS hologram. To see the peaks of the rocking curve better, its plots are zoomed in 21 and 22. To compare

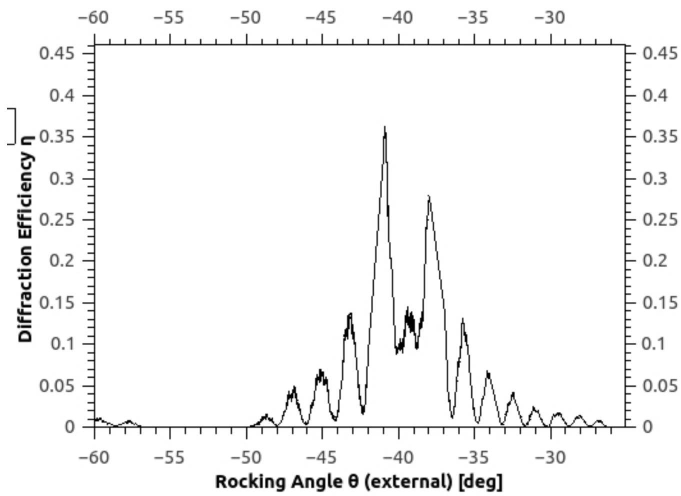

Figure 21: SPPS hologram: -1st order rocking curve (which is zoomed in) as the function of external angle (measured in 2020).

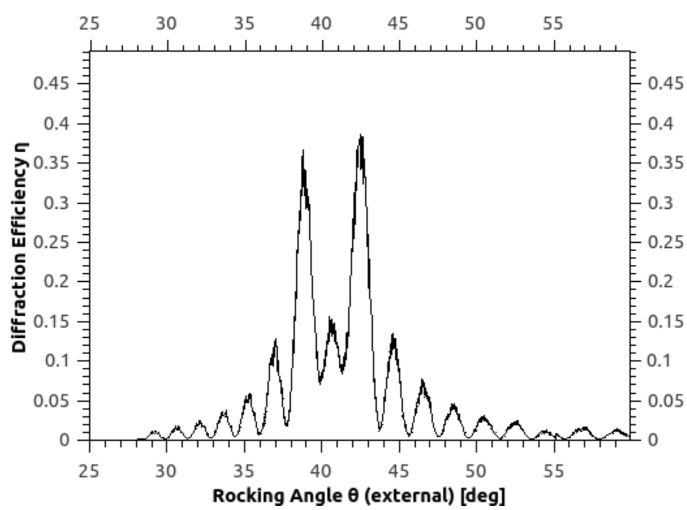

Figure 22: SPPS hologram: $+1$st order rocking curve (which is zoomed in) as the function of external angle (measured in 2020).

the experimental and fit data of SPPS hologram, the same Mathematica program was used which is shown in Fig. 23. According to the fit, the amplitude of the spatial modulation of the refractive index, the effective thickness and the grating spacing for this hologram are: 0.0166 ± 0.0043, 30.9 ± 5.3 μm and 492.26100 ± 0.00331 nm, respectively. This sample consists of two photopolymer layers which are put together one after another. The result is meaningful: n_1 is comparable to the PS results and to what is stated here [5]. The reason could be that some undesirable processes such as: absorption, shrinkage or scattering happened during the recording process because of the large thickness. Note also that the minima neighboring the central maximum do not reach $\eta = 0$, which is also a hint that the grating strength is not constant throughout the full sample thickness, but decreases. The thickness parameter ρ for SPPS hologram equals to $199,22$ which is larger than 10. Here it seems that the DE of 1st order is higher than the -1st order. So we should check also the Q' parameter from Eq. (18).

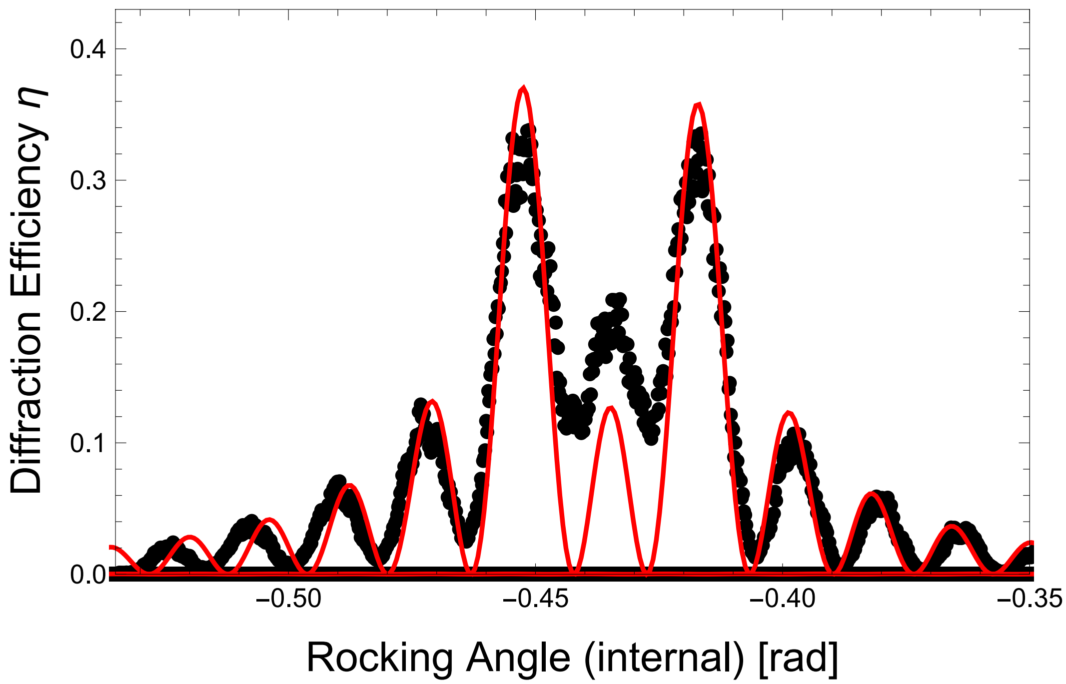

Figure 23: SPPS hologram: experimental data (black points) and fit data (solid red curve). In measuring of this sample, no higher Bragg orders were seen. By substituting the values of Λ and λ we get $\sin\theta_B^{ext} > 1$ which is impossible.

4.3 Two Photopolymer Layer Hologram (PSPS)

The grating is structured as described in Sec. 3.2.4 and sketched in Fig. 9. The measured DEs of the $\pm$1st Bragg diffraction orders and the forward diffracted light are shown in Fig. 25. It is obvious that its angular dependency is completely different from that of the PS or SPPS holograms. There are actually two separate gratings that are glued together at the constant distance (thickness of substrate of foil), therefore the transfer matrix implementation for so-called multilayer holograms will be used as explained below (cf. [1, 24]). The DE of this hologram at $\pm$1st orders is about 0.4 and higher than the SPPS hologram. As the sample rotates and goes far from the Bragg angles, the groups of oscillations appear. Each oscillation is not a single peak but consists of series of local maxima which may be asymmetric and have various heights. Again here in comparison to the PS hologram the minima of the DE of some oscillations do not reach the zero point maybe because of the absorption in the grating. The latter is, again, twice the thickness of a single-foil grating. As mentioned above, the PSPS hologram is a nonuniform multilayer hologram because there is a substrate between two photopolymers whose angular selectivity has series of local maxima and minima. We used a

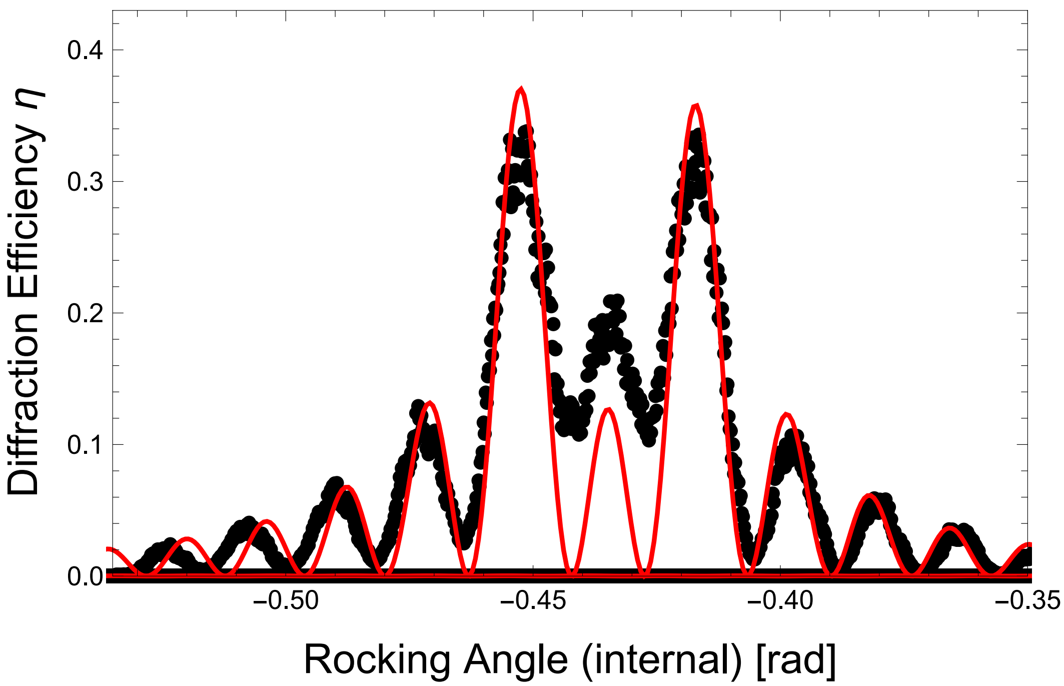

Figure 24: SPPS hologram: experimental data (black points) and fit data (solid red curve). In measuring of this sample, no higher Bragg orders were seen. By substituting the values of Λ and λ we get $\sin\theta_B^{ext} > 1$ which is impossible.

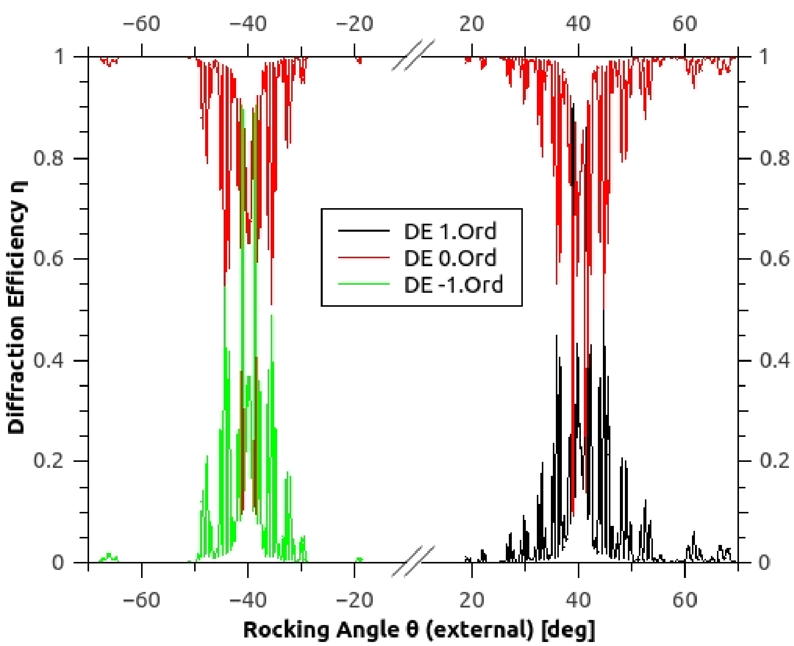

Figure 25: PSPS hologram: -1st, 0th and $+1$st order rocking curves (green, red and black curves, respectively) as the function of external angle (measured in 2020).

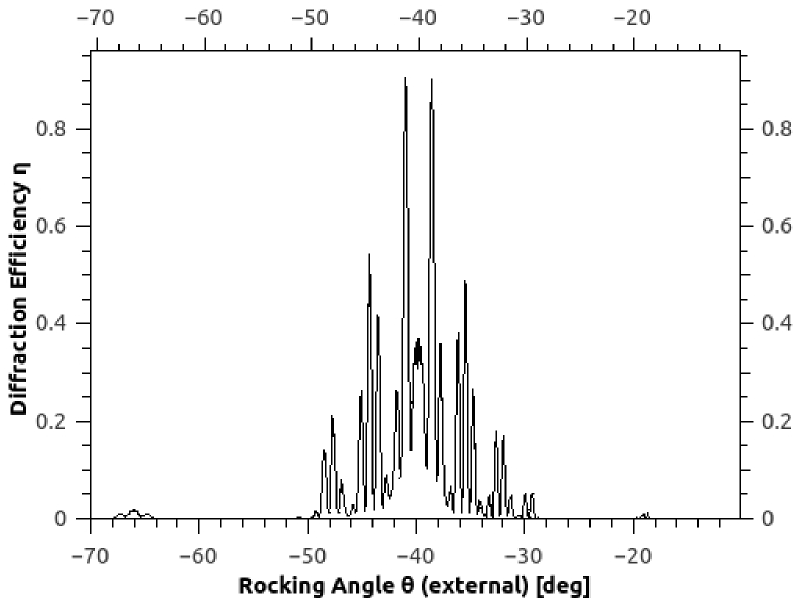

Figure 26: PSPS hologram: −1st order rocking curve (zoomed in) as the function of external angle (measured in 2020).

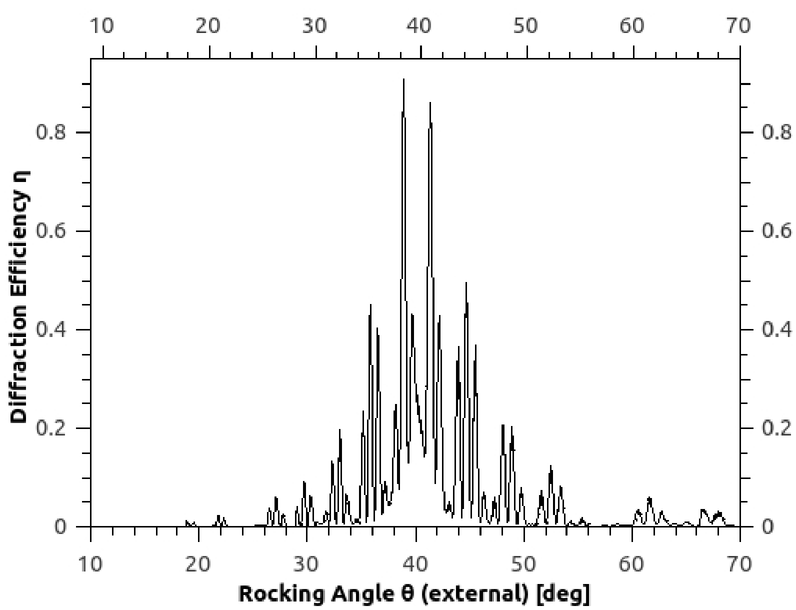

Figure 27: PSPS hologram: +1st order rocking curve (zoomed in) as the function of external angle (measured in 2020).

simulation for DE of the multilayer volume holographic gratings instead of fitting, because it was very difficult to detect all the diffraction points around the ±1st diffraction orders due to the high number of oscillations and it seems some of them are missed. Beacause of the lack of some data, no fitting was performed. To characterize the properties of the multilayar hologram, the output wave was determined by multiplying the transfer matrices for each layer (cf. [1, 24]). According to the Kogelnik theory the reconstruction and reconstructed beams, R and S, are given by (29) and (30), respectively. The transfer matrix for the hologram is written in the following way

$$M = \begin{pmatrix} \left(\cos\phi + i\frac{\xi \sin\phi}{\phi}\right) e^{-i\xi} & -i\frac{\nu \sin\phi}{\phi} e^{-i\xi} \\ -i\frac{\nu \sin\phi}{\phi} e^{-i\xi} & \left(\cos\phi - i\frac{\xi \sin\phi}{\phi}\right) e^{-i\xi} \end{pmatrix}, \tag{45}$$

where

$$\phi = \sqrt{\xi^2 + \nu^2}\,. \tag{46}$$

The transfer matrix for the substrate with the thickness t is as follows if it is assumed that the refractive index of the substrate is equal to the average of the refractive index of the hologram (1.505)

$$D = \begin{pmatrix} 1 & 0 \\ 0 & \exp\left[-i\frac{\Delta\theta K \sin(\theta_K - \theta_B) t}{\cos\theta}\right] \end{pmatrix} = \begin{pmatrix} 1 & 0 \\ 0 & \exp\left[-i\frac{t(\theta - \theta_B) K \cos\theta_B}{\cos\theta}\right] \end{pmatrix}. \tag{47}$$

The transfer matrix of the whole structure of a nonuniform hologram without absorption will be achieved by multiplication of the transition matrices of all the layers

$$\begin{pmatrix} R_{out} \\ S_{out} \end{pmatrix} = M_1 \times D_1 \times M_2 \times D_2 \times \begin{pmatrix} 1 \\ 0 \end{pmatrix}. \tag{48}$$

To analyze the multilayer hologram, a theory curve was plotted according to the calculated diffraction efficiency and the measured data was compared with the theory curve (see Fig. 28 and 29). The appropriate model would be Rigorous Coupled-Wave Analysis (RCWA) [21] combined with the matrix theory. The RCWA method can be used to analyze the diffraction of gratings surrounding by two different materials. It is possible but hard to realize. It can be computed in a reasonable time.

4.4 Neutron Diffraction from the Holograms

The recorded holograms can be used also for diffraction of neutrons. Two holograms: SPPS and PSPS holograms were measured with neutrons at the very-cold neutron beam line PF2 VCN at Laue Langevin in Grenoble, France. The rocking curve of ±1st orders of SPPS hologram are shown in Fig. 30. The absolute angular values are arbitrary. We cannot check for normal incidence but we can estimate the ±1st Bragg orders. From Bragg's law

$$\sin\theta_B^N = \frac{\lambda}{2\Lambda} \approx 0.005\,, \tag{49}$$

where θ_B^N is the Bragg angle for neutron. The angle of diffracted neutron beam is too small, therefore

$$\sin\theta_B^N \approx \theta_B^N \approx 0.005\ rad \approx 0.29^\circ\,, \tag{50}$$

According to the Bragg's law, the DE at this position is about 0.06. It is difficult to fit the data for neutron beacause the neutron has a very broad wavelength distribution [17, 23]. To

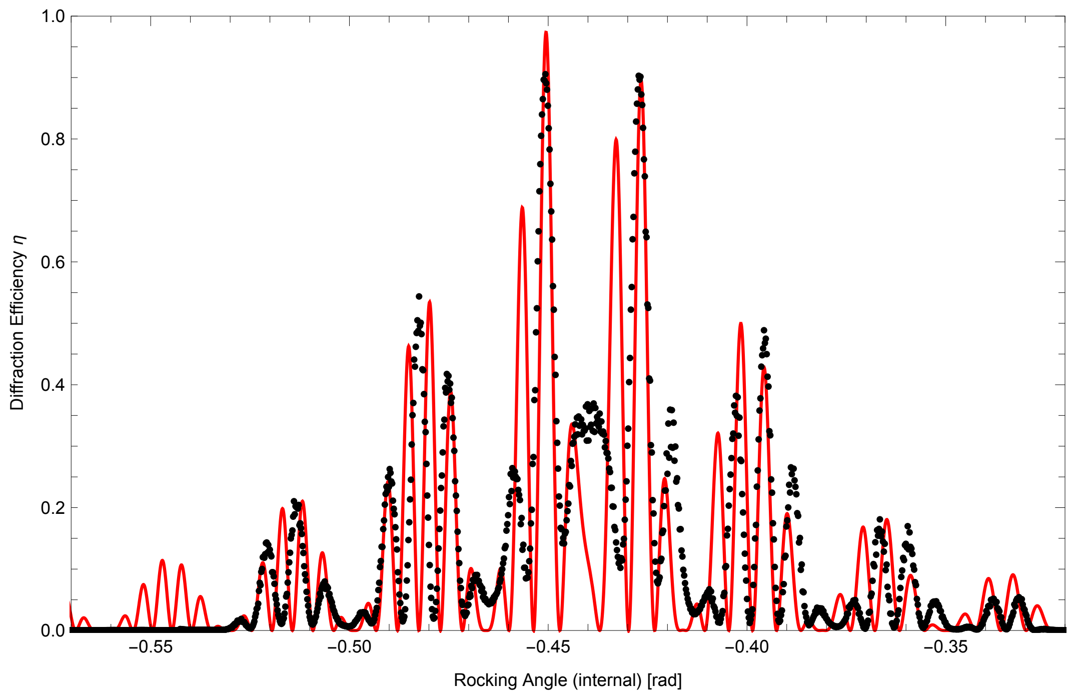

Figure 28: PSPS hologram: -1st order, experimental data (black points) and theory curve (red solid curve). As it is shown, the angular selectivity of this hologram has series of local maxima and minima. Here the theory curve of a nonuniform multilayer hologram was plotted with the following parameters: thickness of each photopolymer: 16 μm, thickness of substrate: 50 μm, $\lambda = 633$ nm, $n_1 = 0.008$, $\Lambda = 487$ nm.

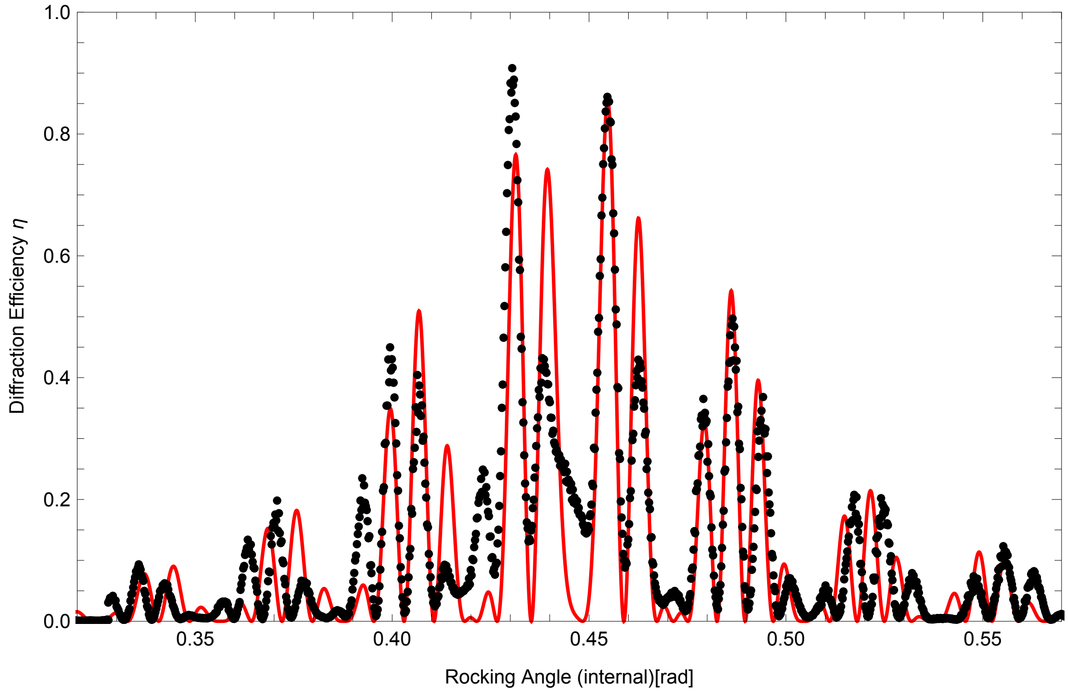

Figure 29: PSPS hologram: +1st order, experimental data (black points) and theory curve (red solid curve). The theory curve for the +1st order was plotted with the same parameters for -1st order but for the opposite angles: thickness of each photopolymer: 16 μm, thickness of substrate: 50 μm, $\lambda = 633$ nm, $n_1 = 0.008$, $\Lambda = 487$ nm.

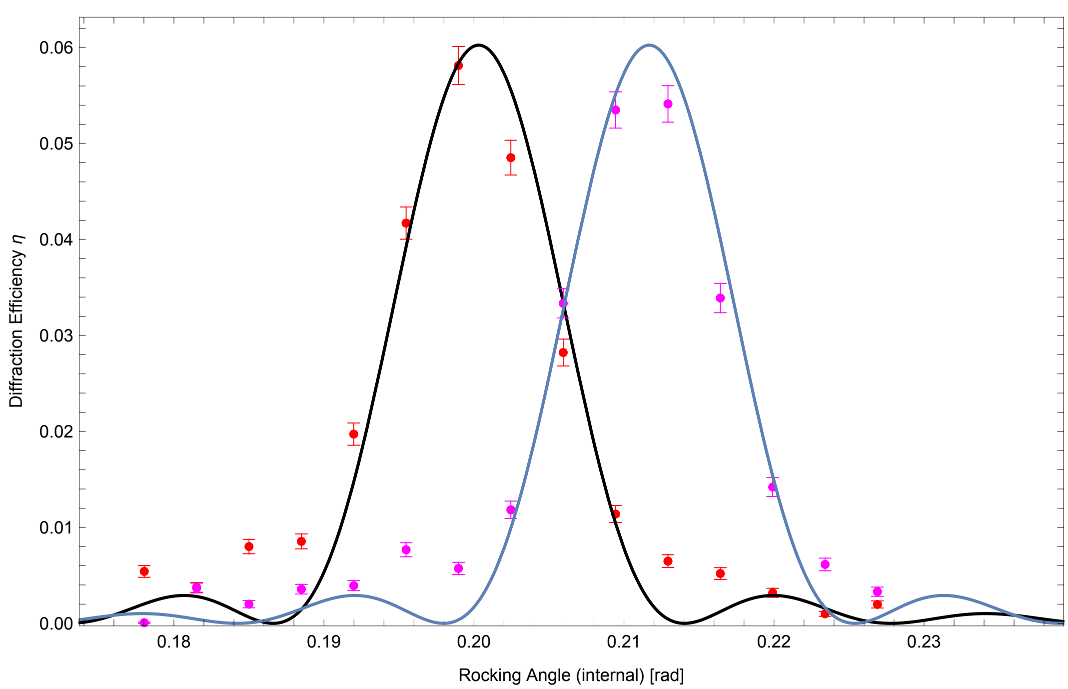

Figure 30: SPPS hologram: experimental data (red (-1st order) and pink points (+1st order)) and theory curves (solid black (-1st order) and blue curves (+1st order).

see the difference between the experimental data and the theory curve, the measured rocking curve was plotted on the Kogelnik theory curve. The neutron DE has the similar form as Eq. (35) but the ν and ξ are replaced by (cf. [16])

$$\nu = \frac{\lambda d b_c \Delta\rho}{2\cos\theta}\,, \tag{51}$$

$$\xi = \frac{\pi d(\theta_B - \theta)}{\Lambda}\,. \tag{52}$$

Here b_c is the coherent scattering length and $\Delta\rho$ is the modulation of the density of material. We should consider that neutron is a fermion and we should solve the Schrödinger equation

$$\Delta\Psi + k^2\Psi = 0\,, \tag{53}$$

with

$$k = n_n\frac{2\pi}{\lambda}\,, \tag{54}$$

where $n_n \approx 1$ is the refractive index for neutron, $\lambda \approx 5$ nm is the mean wavelength of neutron, To plot the theory curve, the approximated values for $\lambda \simeq 5$ nm and $b_c\Delta\rho \simeq 3\ \mu\text{m}^{-2}$ were used to match the height of DE. To calculate the $b_c\Delta\rho$ from (32), we put the maximum value of DE from Fig. 30 in Eq. (35)

$$\sin^2\left(\frac{\lambda d b_c \Delta\rho}{2\cos\theta_B}\right) \approx 0.6\,. \tag{55}$$

Because the diffraction angle for neutron is very small: $\cos\theta_B \approx 1$. Therefore

$$\eta = \sin^2\left(\frac{\lambda d b_c \Delta\rho}{2}\right) \approx 0.6\,. \tag{56}$$

By inserting the values of λ and d in above equation, we get $b_c\Delta\rho \approx 3\ \mu\text{m}^{-2}$.

As it is shown in Fig. 30, the rocking curve of $\pm$1st Bragg orders are overlapped on each other, it means that it does not follow the assumption of Kogelnik theory because this theory is valid only when we have just one Bragg order. The local minima around $\pm$1st orders do not reach the zero point. It is attributed to the wide range wavelength of neutron. When the neutrons with different wavelengths strike the grating, all the parameters depending on the λ will change. But the difference between the wavelengths is small, so the changes in parameters can be also small. In comparison to the results from laser measurements, here the Bragg angles are too small as expected and the $\pm$1st orders are very close to each other. The mean wavelength of neutron (5 nm) is too small in comparison to the laser we used (633 nm). According to the Bragg equation, the Bragg angle depends on the wavelength. If the wavelength decreases, the smaller Bragg angle we will have.

In Fig. 31 and Fig. 32 the data of the measurements are plotted together with the theory curve. For the theory curve, the transmission matrix for this grating was calculated to figure out the amplitude of reconstructed beam by using the approximated parameters $\lambda \simeq 5nm$ and $b_c\Delta\rho \simeq 3\ \mu m^{-2}$ [17]. The rocking curves of $\pm$1 st orders consist of several local maxima and the local minima do not reach the zero point. One can see the angles are too small and the Bragg angles are close to each other. The theory curve did not agree with the data exactly because of the wide wavelength distribution of neutron. The RCWA theory combining with the transmission matrix for multilayer hologram may be a possible solution for fitting or even for a theory curve but it exceeds the scope of this thesis.

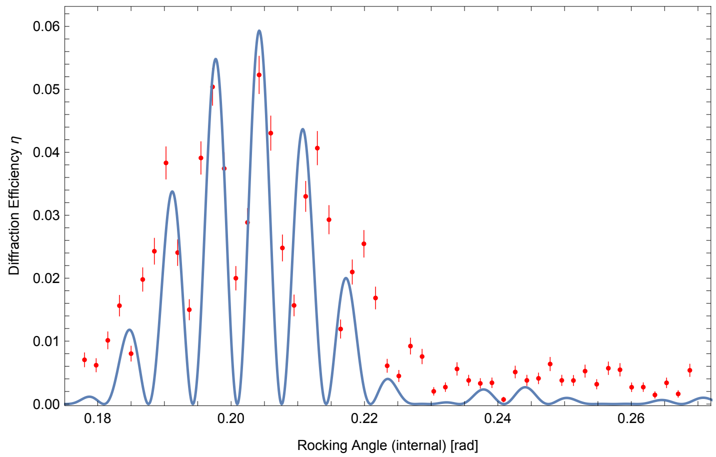

Figure 31: PSPS hologram: diffraction efficiency of −1st order measured with neutrons (red points with red error bars) and the Kogelnik theory curve (blue solid curve).

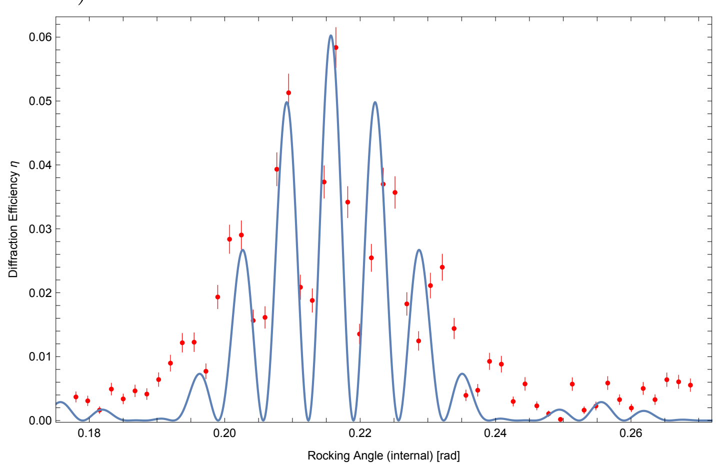

Figure 32: PSPS hologram: diffraction efficiency of +1st order measured with neutrons (red points with red error bars) and the Kogelnik theory curve (blue solid curve).

5 Conclusion

The aim of this master thesis was to record the holograms with one and two layers on the photosensitive material and investigate the properties of the holograms such as their efficiency of converting light into the useful reconstructed wave (diffraction efficiency) and the angular dependency of this diffraction efficiency.

To characterize the holograms, a Mathematica program was used to fit the data. The Kogelnik theory was applied as the fitting model. The best coincidence of the fit and experimental data for PS hologram yields: $n_1 = 0.015100 \pm 0.000025$, $\Lambda = 493.321000 \pm 0.000017$ nm and the effective thickness of this hologram is $d = 15.652 \pm 0.016$ μm.

For SPPS hologram, the amplitude of the spatial modulation of the refractive index, the effective thickness and the grating spacing are: 0.0166 ± 0.0043, 30.9 ± 5.3 μm and 492.26100 ± 0.00331 nm

The PSPS hologram is a nonuniform hologram because there is a substrate between two photopolymers. It was very difficult to measure the Bragg diffractions of this hologram because some of the oscillations did not strike the photodiode while the sample was rotating. To compare the measured diffraction efficiency with the theory, the transmission matrix of the whole hologram was calculated to get the amplitude of the reconstructed beam and the diffraction efficiency. Then the theory curve was plotted and the data was put on the theory to see the difference between them.

If we compare the one layer hologram with two layer holograms, we can see that the diffraction efficiency decreases when the number of photopolymer layer increases. The SPPS and PSPS holograms have more oscillations around the $\pm$1st orders because they are actually made of two holograms. There is a difference between these two holograms namely in PSPS hologram each diffraction point is not a single peak and has several peaks. The combing of RCWA theory with simulations for multilayer holograms could be an appropriate method to characterize the PSPS hologram.

The measurements of the holograms were done two times in a period of about one year. However none of the curing methods was used to fix the holograms, they remained on the photopolymer without any changes and their diffraction efficiencies after one year were as high as the first experiment. It means the Bayfol foils can keep the hologram for a long time.

Abstract

To record diffraction gratings on photosensitive material (Bayfol HX 200), a Mach Zehnder interferometer is constructed as the setup. The samples are foil stacks formed from 1 or 2 photopolymer layers. In this setup, the green laser beam with 514 nm wavelength is used to record the holograms on the photosensitive foils. After recording, the holograms will be read out by a red laser beam with 633 nm wavelength to characterize the quality and properties of the gratings such as angular dependence of the diffraction efficiency with varying number of layers, thickness of grating, grating spacing and the amplitude of the spatial modulation of the refractive index.

Zusammenfassung

Um ein Beugungsgitter in photosensitives Material einzuschreiben, wird ein Mach-Zehnder-Interferometer als Aufbau verwendet. Die Proben sind Folien, die aus 1 oder 2 Photopolymer-Schichten bestehen. In diesem Aufbau wird der grüne Laserstrahl mit 514 nm Wellenlänge verwendet, um Hologramme auf den lichtempfindlichen Folien einzuschreiben. Nach dem Einschreiben werden die Hologramme von einem roten Laserstrahl mit 633 nm Wellenlänge ausgelesen, um die Qualität und Eigenschaften von Gittern wie die Winkelabhängigkeit der Beugungseffizienz bei variierender Anzahl von Schichten, Brechungsindex-Modulation, Gitterkonstante und Dicke zu charakterisieren.

References

[1] L. Au, J. Newell, and L. Solymar. Non-uniformities in thick dichromated gelatin transmission gratings. *Journal of Modern Optics*, 34(9):1211–1225, 1987.

[2] H. Berneth, F. K. Bruder, T. Fäcke, R. Hagen, D. Hönel, D. Jurbergs, T. Rölle, and M.-S. Weiser. Holographic recording aspects of high-resolution Bayfol HX photopolymer. In H. I. Bjelkhagen, editor, *Practical Holography XXV: Materials and Applications*, volume 7957, pages 122 – 136. International Society for Optics and Photonics, SPIE, 2011.

[3] F.-K. Bruder, H. Bang, T. Fäcke, R. Hagen, D. Hönel, E. Orselli, C. Rewitz, T. Rölle, D. Vukicevic, and G. Walze. Precision holographic optical elements in Bayfol HX photopolymer. In H. I. Bjelkhagen and V. M. B. Jr., editors, *Practical Holography XXX: Materials and Applications*, volume 9771, pages 8 – 28. International Society for Optics and Photonics, SPIE, 2016.

[4] F.-K. Bruder, F. Deuber, T. Fäcke, R. Hagen, D. Hönel, D. Jurbergs, T. Rölle, and M.-S. Weiser. Reaction-diffusion model applied to high resolution Bayfol HX photopolymer. In H. I. Bjelkhagen and R. K. Kostuk, editors, *Practical Holography XXIV: Materials and Applications*, volume 7619, pages 145 – 159. International Society for Optics and Photonics, SPIE, 2010.

[5] F.-K. Bruder, T. Fäcke, R. Hagen, D. Hönel, E. Orselli, C. Rewitz, T. Rölle, and G. Walze. Diffractive optics with high Bragg selectivity: volume holographic optical elements in Bayfol® HX photopolymer film. In L. Mazuray, R. Wartmann, and A. P. Wood, editors, *Optical Systems Design 2015: Optical Design and Engineering VI*, volume 9626, pages 186 – 194. International Society for Optics and Photonics, SPIE, 2015.

[6] Coherent. Data sheet genesis mx slm-series. https://www.coherent.com/lasers/laser/genesis-mx-slm-series. Accessed 29-March-2021.

[7] N. Company. Fundamentals of spatial filtering. https://www.newport.com/n/spatial-filters. Accessed 08-March-2021.

[8] J. Eichler and G. Ackermann. *Grundlagen der Holographie*, pages 9–30. Springer Berlin Heidelberg, Berlin, Heidelberg, 1993.

[9] M. Fally, J. Klepp, and Y. Tomita. An experimental study on the validity of diffraction theories for off-bragg replay of volume holographic gratings. *Applied Physics B*, 108(1):89–96, 2012.

[10] D. Gabor. Microscopy by reconstructed wave-fronts. *Proceedings of the Royal Society of London. Series A. Mathematical and Physical Sciences*, 197(1051):454–487, jul 1949.

[11] T. K. Gaylord and M. G. Moharam. Thin and thick gratings: terminology clarification. *Appl. Opt.*, 20(19):3271–3273, Oct 1981.

[12] J. Goodman. *Introduction to Fourier Optics*. McGraw-Hill, New York, 1996.

[13] E. Hecht. *Optics, Global Edition*. Pearson Education Limited, 2016.

[14] R. V. Johnson and A. R. Tanguay. Stratified volume holographic optical elements. *Opt. Lett.*, 13(3):189–191, Mar 1988.

[15] D. Jurbergs, F.-K. Bruder, F. Deuber, T. Fäcke, R. Hagen, D. Hönel, T. Rölle, M.-S. Weiser, and A. Volkov. New recording materials for the holographic industry. In H. I. Bjelkhagen and R. K. Kostuk, editors, *Practical Holography XXIII: Materials and Applications*, volume 7233, pages 149 – 158. International Society for Optics and Photonics, SPIE, 2009.

[16] J. Klepp, C. Pruner, M. Ellabban, Y. Tomita, H. Lemmel, H. Rauch, and M. Fally. Neutron-optical gratings from nanoparticle-polymer composites. *Nuclear Instruments and Methods in Physics Research Section A: Accelerators, Spectrometers, Detectors and Associated Equipment*, 634(1, Supplement):S59 – S62, 2011. Proceedings of the International Workshop on Neutron Optics NOP2010.

[17] J. Klepp, C. Pruner, Y. Tomita, P. Geltenbort, J. Kohlbrecher, and M. Fally. Advancing data analysis for reflectivity measurements of holographic nanocomposite gratings. *Journal of Physics: Conference Series*, 746:012022, sep 2016.

[18] H. Kogelnik. Coupled wave theory for thick hologram gratings. *The Bell System Technical Journal*, **48**(9):2909–2947, Nov 1969.

[19] R. K. Kostuk. *Holography: Principles and Applications.* CRC Press, 2019.

[20] T. H. Maiman. Stimulated optical radiation in ruby. *Nature*, 187(4736):493–494, 1960.

[21] M. G. Moharam, E. B. Grann, D. A. Pommet, and T. K. Gaylord. Formulation for stable and efficient implementation of the rigorous coupled-wave analysis of binary gratings. *J. Opt. Soc. Am. A*, 12(5):1068–1076, May 1995.

[22] G. P. Nordin, R. V. Johnson, and A. R. Tanguay. Diffraction properties of stratified volume holographic optical elements. *J. Opt. Soc. Am. A*, 9(12):2206–2217, Dec 1992.

[23] T. Oda, M. Hino, M. Kitaguchi, H. Filter, P. Geltenbort, and Y. Kawabata. Towards a high-resolution tof-mieze spectrometer with very cold neutrons. *Nuclear Instruments and Methods in Physics Research Section A: Accelerators, Spectrometers, Detectors and Associated Equipment*, 860:35–41, 2017.

[24] E. F. Pen and M. Y. Rodionov. Properties of multilayer nonuniform holographic structures. *Quantum Electronics*, **40**(10):919–924, Dec 2010.

[25] N. Uchida. Calculation of diffraction efficiency in hologram gratings attenuated along the direction perpendicular to the grating vector. *J. Opt. Soc. Am.*, 63(3):280–287, Mar 1973.